



**TURUN
YLIOPISTO**
UNIVERSITY
OF TURKU

PHYSICOCHEMICAL PROPERTIES AND CHARACTERIZATION OF BIOCERAMICS AND BIOACTIVE GLASSES FOR BONE REPAIR

Saara V. Sirkiä



**TURUN
YLIOPISTO**
UNIVERSITY
OF TURKU

PHYSICOCHEMICAL PROPERTIES AND CHARACTERIZATION OF BIO-CERAMICS AND BIOACTIVE GLASSES FOR BONE REPAIR

Saara V. Sirkiä

University of Turku

Faculty of Medicine
Institute of Dentistry
Biomaterials Science
Finnish Doctoral Programme in Oral Sciences (FINDOS-Turku)
Turku Clinical Biomaterial Centre - TCBC

Supervised by

Professor Pekka Vallittu, DDS, PhD
Institute of Dentistry
Department of Biomaterials Science and
Turku Clinical Biomaterial Centre TCBC
University of Turku
Turku, Finland

Adjunct professor Terhi Heino, MSc,
PhD
Institute of Biomedicine
University of Turku
Turku, Finland

Reviewed by

Professor Wei Xia
Applied Materials Science
Department of Materials Science and
Engineering
University of Uppsala
Uppsala, Sweden

Professor Jonathan Massera
Faculty of Medicine and Health
Technology
Tampere University
Tampere, Finland

Opponent

Professor Juha Tuukkanen
Department of Anatomy and Cell Biology
Translational Medicine Research Unit
University of Oulu
Oulu, Finland

The originality of this publication has been checked in accordance with the University of Turku quality assurance system using the Turnitin OriginalityCheck service.

ISBN 978-951-29-9525-7 (PRINT)
ISBN 978-951-29-9526-4 (PDF)
ISSN 0355-9483 (Print)
ISSN 2343-3213 (Online)
Painosalama, Turku, Finland 2023

“Storms probably exist only because
after them we can have a sunrise”
-Tove Jansson

To my family and friends

UNIVERSITY OF TURKU

Faculty of Medicine

Institute of Dentistry

Biomaterials Science

SAARA VILHELMIINA SIRKIÄ: Physicochemical properties and characterization of bioceramics and bioactive glasses for bone repair

Doctoral Dissertation, 106 pp.

Finnish Doctoral Programme in Oral Sciences – FINDOS Turku

November 2023

ABSTRACT

Different materials *i.e.* natural bone and synthetic biomaterials have been widely used to improve bone repair and regeneration. Even though there is a long tradition in studying and developing various biomaterials, more research is still needed. The aim of this thesis was to compare the physicochemical properties of commonly used bioceramics (hydroxyapatite, carbonate apatite, alumina) and bioactive glasses (45S5, S53P4) and to physicochemically and biologically characterize two new bioceramics in the field of bone repair (silica-modified alumina and functionalized calcium carbonate, FCC).

Physicochemical properties were characterized by various methods. Attenuated Total Reflectance Fourier Transform Infrared (ATR-FTIR) was used to analyze biomaterials' vibrational features, while the crystal structure was analyzed by X-Ray power Diffraction (XRD) and biomaterials' morphology and elemental contents were evaluated by Scanning Electron Microscopy – Energy-Dispersive X-ray Analysis (SEM-EDXA). Dissolution behavior of the biomaterials in terms of ion release and pH change was characterized in a static or in a continuous flow-through method in Tris buffer, simulated body fluid or cell culture medium. The used dissolution methods were selected based on chemical composition of the materials. The biomaterials were biologically characterized by evaluating the viability of pre-osteoblastic MC3T3-E1 cells by WST method, when cells were cultured in the presence of biomaterials. SEM and TEM were also used to evaluate cell morphology in the presence of functionalized calcium carbonate.

All biomaterials, which were characterized in this thesis differed in their physicochemical properties, such as releasing ions and causing a pH change. Even though minor quantities of silica were detected to dissolve from silica-modified alumina particles, no effect on pre-osteoblast cell viability was detected. However, FCC was shown to reduce the viability of pre-osteoblasts, which probably was caused by FCC's ability to adsorb calcium ions and proteins from cell culture medium. In this thesis, it was shown that these biomaterials differ from each other based on their physicochemical properties, which are considered to be important for suitability in a biological settings. These properties might also affect the choice of an optimal biomaterial for bone repair.

KEYWORDS: physicochemical characterization, ion-release, bioactive glass, bioceramics, osteoblast, bone repair

TURUN YLIOPISTO

Lääketieteellinen tiedekunta

Hammaslääketieteen laitos

Biomateriaalitiede

SAARA VILHELMIINA SIRKIÄ: Luun korjaukseen soveltuvien biokeraamien ja bioaktiivisten lasien fysikokemialliset ominaisuudet ja karakterisointi

Väitöskirja, 106 s.

Kansallinen suun terveystieteiden tohtoriohjelma (FINDOS-Turku)

Marraskuu 2023

TIIVISTELMÄ

Luun korjauksessa käytetään niin biologista luuta kuin synteettisiä biomateriaalejakin. Vaikka luun täytemateriaaleja on kehitetty ja tutkittu laajasti, uusia tutkimustuloksia materiaaleista, niiden ominaisuuksista ja kliinisestä soveltuvuudesta tarvitaan yhä. Tämän väitöskirjan tarkoituksena oli vertailla fysikokemiallisesti kliinisesti käytettyjä biokeraameja (hydroksiapatiitti, karbonoitu apatiitti, alumiinioksidi) ja bioaktiivisia laseja (45S5, S53P4), sekä karakterisoida fysikokemiallisesti ja biologisesti kahta biomateriaalia, joita ei aiemmin ole tutkittu luun täyteenä (piipinnoitettu alumiinioksidi ja funktionalisoitu kalsium karbonaatti, FCC).

Biomateriaalien ominaisuuksia karakterisoitiin useilla eri menetelmillä. Materiaalien molekyylien välisiä sidoksia tutkittiin ATR-FTIR-spektroskopiolla ja materiaalien kolmiulotteista rakennetta ja kiteisyyttä röntgenkristallografialla (XRD). Biomateriaalipartikkelien morfologiaa ja alkuainepitoisuuksia tutkittiin pyyhkäisyelektronimikroskopiolla ja energia-dispersiivisellä röntgenspektroskopiolla (SEM-EDXA). Biomateriaalien liukenemiskäyttäytymistä, kuten ionien vapautumista ja biomateriaalien kykyä muuttaa ympäristön pH:ta tutkittiin eri menetelmillä riippuen materiaalien ominaisuuksista, joko staattisessa tai jatkuvan läpivirtauksen systeemissä Tris-puskurissa, simuloitussa kudostesteessä (SBF) tai solujen kasvatusaineessa (medium). Biologisessa karakterisoinnissa tutkittiin pre-osteoblastien elinkykyä, kun niitä kasvatettiin biomateriaalien läsnä ollessa. SEM- ja TEM-kuvaustekniikkaa käytettiin solujen morfologian arvioitiin, kun soluja oli kasvatettu FCC-biomateriaalin läsnä ollessa.

Kaikki tutkitut biomateriaalit erosivat toisistaan fysikokemiallisilta ominaisuuksiltaan. Pii-pinnoitetun alumiinioksidin ei havaittu vaikuttavan pre-osteoblastien elinkykyyn, vaikka vähäisiä pitoisuuksia piitä havaittiinkin liukenevan solujen kasvatusmediumiin. Toisaalta FCC-materiaali heikensi huomattavasti pre-osteoblastien elinkykyä, mikä mahdollisesti aiheutui materiaalin kyvystä adsorboida kalsiumioneja ja seerumin proteiineja mediumista, ja siten vaikuttaen epäsuorasti solujen elinkykyyn. Tutkimuksessa saavutetuilla tuloksilla materiaalien erilaisista ominaisuuksista on merkitystä pohdittaessa materiaalien biologista soveltuvuutta ja valittaessa optimaalista biomateriaalia kliiniseen käyttöön luun korjautumisen ja uudistumisen tehostamiseksi.

AVAINSANAT: fysikokemiallinen karakterisointi, ionien vapautuminen, bioaktiivinen lasi, osteoblasti, luun korjaus

Table of Contents

Abbreviations	8
List of Original Publications	9
1 Introduction	10
2 Review of the Literature	12
2.1 Biomaterials in bone repair and replacement	12
2.1.1 Bone structure and functions.....	12
2.1.2 Bone development and repair	13
2.1.3 Repairing the bone defects with biomaterials	16
2.1.3.1 Biomechanical and topographical properties of biomaterials.....	19
2.1.3.2 Effects of ions released from biomaterials	19
2.2 Ceramics and glasses as biomaterials	20
2.2.1 Biostable materials.....	23
2.2.1.1 Alumina	23
2.2.1.2 Zirconia.....	23
2.2.2 Bioresorbable materials.....	24
2.2.2.1 Tricalcium phosphates.....	24
2.2.2.2 Hydroxyapatite.....	24
2.2.2.3 Carbonated apatite	24
2.2.2.4 Calcium carbonate.....	25
2.2.2.5 Bioactive glasses.....	25
2.2.3 Surface-modified materials.....	28
2.3 In vitro characterization of biomaterials	29
2.3.1 Physicochemical and surface characterization	29
2.3.2 Biological characterization.....	31
3 Aims	33
4 Materials and Methods	34
4.1 Biomaterials and reagents.....	34
4.2 Physicochemical characterization	36
4.2.1 ATR-FTIR analysis (I–III).....	36
4.2.2 XRD analysis (I–III)	36
4.2.3 SEM-EDX analysis (I–III).....	36
4.2.4 pH change and ion release (I–III)	37
4.2.4.1 pH changes and ion release in continuous dynamic system in vitro (I–III)	37

4.2.4.2	pH change and ion release in static in vitro system with SBF, Tris buffer and α MEM (II).....	40
4.2.4.3	pH changes and ion release (III).....	40
4.3	Biological characterization.....	41
4.3.1	Cell cultures (II–III).....	41
4.3.2	MC3T3-E1 cell viability with biomaterials (II–III).....	41
4.3.3	SEM and TEM imaging of MC3T3-E1 cells (III).....	42
4.4	Statistical analysis (I–III).....	43
5	Results	44
5.1	Physicochemical characterization of biomaterials (I–III).....	44
5.1	Biological characterization of biomaterials (II–III).....	55
6	Discussion	59
7	Conclusions	66
	Acknowledgements	67
	References	69
	Original Publications	77

Abbreviations

ATR-FTIR	Attenuated Total Reflectance Fourier Transform Infrared
BG	Bioactive glass
CAP	Carbonate apatite
FBS	Fetal bovine serum
HAP	Hydroxyapatite
ICP-OES	Inductively Coupled Plasma Optical Emission Spectrometry
MSC	Mesenchymal stem cell
SBF	Simulated body fluid
SEM-EDXA	Scanning Electron Microscopy – Energy-Dispersive X-ray Analysis
TEM	Transmission electron microscopy
Tris	2-amino-2-hydroxymethyl-propane-1,3-diol
XRD	X-Ray power Diffraction

List of Original Publications

This dissertation is based on the following original publications, which are referred to in the text by their Roman numerals:

- I Saara V. Sirkiä, Miho Nakamura, Syeda Qudsia, Minna Siekkinen, Jan-Henrik Smått, Jouko Peltonen, Terhi J. Heino, Leena Hupa, Pekka K. Vallittu. Structural and elemental characterization of glass and ceramic particles for bone surgery. *Dental Materials*. 2021 Sep. 37(9):1350–1357.
- II Saara V. Sirkiä, Minna Siekkinen, Syeda Qudsia, Jan-Henrik Smått, Jouko Peltonen, Leena Hupa, Terhi J. Heino, Pekka K. Vallittu. Physicochemical and biological characterization of silica-coated alumina particles. *Dental Materials*. 2022 Dec.38(12):1878–1885
- III Saara V. Sirkiä, Syeda Qudsia, Minna Siekkinen, Wolfgang Hoepfl, Tanja Budde, Jan-Henrik Smått, Jouko Peltonen, Leena Hupa, Terhi J. Heino, Pekka K. Vallittu. Physicochemical and biological characterization of functionalized calcium carbonate. *Materialia*. 2023 Mar. 28:101742.

The original publications have been reprinted on the end of this book with the permission of the copyright holders. All three publications (I–III) are licensed under CC BY 4.0 (<https://creativecommons.org/licenses/by/4.0/>).

1 Introduction

Novel bone replacing materials are currently more widely required due to increased aging population and various diseases and traumas affecting bone tissue and thus the quality of life (Hench, 2009; Shanmugam & Sahadevan, 2018). For these requirements, many various bone substitute materials have been developed. These materials consist of various material groups, but each must be biocompatible, adapt into the implantation site and replace the properties of lost tissue. In addition, bone substitute material should not cause harmful effects, such as foreign body reactions, infections, tumorigenesis, toxicity or hypersensitivity.

Various bone substitutes of different origins have been used for bone regeneration (Baldwin et al., 2019; W. Wang & Yeung, 2017). A substitute graft from the same individual as the recipient, *i.e.* an autograft, is known as a gold standard material for augmentation. In addition, bone grafts from separate individuals have been used, where allografts are from the same and xenografts from different species than the recipient (Baldwin et al., 2019). In addition, alloplastic or synthetic biomaterials can be used for bone substitution. Alloplastic material is synthetic material, which includes some chemical composition of natural bone, and the synthetic biomaterial can be polyacrylates or ceramics, *e.g.* PMMA or alumina (Shanmugam & Sahadevan, 2018; W. Wang & Yeung, 2017).

Autograft is good material to avoid possible rejection reactions, and it has high osteoinductive, osteoconductive and osteogenic properties. On the other hand, there are drawbacks with autografts, *e.g.* the need for two surgeries, tissue availability, donor site morbidity and possible secondary surgery (Baldwin et al., 2019). Alternatives for autograft are allografts and xenografts, which are ready-to-use and of a better availability, but also have some limitations, *e.g.* the risk of infections and disease transmission (Baldwin et al., 2019; Monchau et al., 2013). Synthetic augmentation materials, alloplastic and synthetic biomaterials form together a larger group of biomaterials, which can be applied as bone-replacing materials. Combining various substitute materials can bring together the best properties of each material and thereby an optimal graft. However, even though the number of substitute materials available for bone replacement has increased in last decades, comparative

research about different substitute materials is weak and also is mainly of a low level and based on individual case series at the time (Baldwin et al., 2019).

Even though the natural augmentation as an allograft is good for bone substitution, there are several limiting factors, as mentioned above. Thus, synthetic augmentation materials have been developed to address these limitations, and to respond to the increased clinical demand for bone filling materials to treat our increasing population (Hoppe et al., 2011; W. Wang & Yeung, 2017). Prerequisites in the development of new biomaterials is the characterization of physiochemical as well as biological properties in order to obtain an implant, which is safe to use and well integrating into the bone tissue. Thus, in this thesis we compared synthetic biomaterials physicochemically and also a new biomaterial in the field of bone repair biologically. This information is needed for the development of biomaterials and for choosing an optimal biomaterial for bone repair.

2 Review of the Literature

2.1 Biomaterials in bone repair and replacement

2.1.1 Bone structure and functions

Bone matrix consists of an inorganic (60% of bone's dry weight) and an organic component (40% of bone's dry weight). The organic phase mostly consists of collagen I, but other collagens (II, III, V, XI) also exist in bone tissue. The inorganic component consists of calcium phosphate mineral, mainly hydroxyapatite ($\text{Ca}_{10}(\text{PO}_4)_6(\text{OH})_2$, HAP) (Table 1). In addition, bone matrix contains numerous growth factors, proteoglycans, phospholipids and various other proteins. The inorganic and organic constituents are combined in bone, when hydroxyapatite crystals are arranged within the collagen fibers during bone formation and mineralization. This structure maximizes the resistance capacity of bone, when hydroxyapatite mainly resists the compressive forces and collagen the stretch forces. (Pan et al., 2010; Safadi et al., 2009).

Table 1. Approximate composition of bone inorganic component. Modified from ref. (Pan et al., 2010).

COMPONENT	MASS%
Ca	26.7
P	12.47
Na	0.731
K	0.055
Mg	0.436
F	0.07
Cl	0.08
CO_3^{2-}	3.48

Bone tissue is constantly renewed, which is necessary because bone is targeted with torsional stress and cyclic loading, without forgetting possible tissue injury. Annually, trabecular bone regenerates 25% and cortical bone 3% of itself. However, similarly to other regenerative processes, bone remodeling capacity also reduces with an increasing age. (Safadi et al., 2009; W. Wang & Yeung, 2017).

The bone cells, *i.e.* osteoblasts, osteocytes and osteoclasts are important in bone maintenance and repair. In early childhood, bone tissue is actively growing to increase bone size and to generate optimal shape. Bone remodeling occurs however, throughout our lifespan via simultaneous processes of bone resorption and formation. These processes maintain bone tissue structure in response to mechanical loading and are essential for the mineral balance of a human body, as calcium is released from or deposited in the bone tissue. (Safadi et al., 2009).

Osteoblasts and osteocytes are derived from mesenchymal stem cells (MSC), unlike osteoclasts, which are derived from hematopoietic stem cells. Osteoblastic cell is responsible for bone matrix formation and mineralization. After osteoblasts have formed bone matrix, part of them differentiate into osteocytes, which are located within the bone matrix, or turn into lining cells, which, as the name implies, are located on bone surfaces. Part of osteoblasts can also disappear through programmed cell death, *i.e.* apoptosis. In adults, the lining cells are mainly inactive, but can be reactivated into functional osteoblasts for new bone formation during fracture repair or remodeling. The osteocyte coordinates bone remodeling via mechanical and hormonal signals to both osteoblasts and osteoclasts, while multinuclear osteoclasts derived from the monocyte/macrophage lineage of hematopoietic stem cells, are responsible for bone resorption. (Bellido et al., 2019; Safadi et al., 2009).

2.1.2 Bone development and repair

Human bones are formed via intramembranous or endochondral bone formation, which differ from each other primarily on whether there is a cartilage formation phase prior to bone formation or not. In the intramembranous or direct bone formation, bone is, as the name implies formed directly without a cartilage interphase. MSCs aggregate and differentiate into osteoblasts and form ossification centers, where the bone is mineralized. In addition, part of osteoblasts differentiates into osteocytes. In the end, bone lamellar structure is formed, and the Haversian remodeling occurs in adults. Intramembranous bone formation occurs in flat bones, such as skull, clavicle and most of the facial bones. (Anna-Marja Säämänen et al., 2022; Safadi et al., 2009).

Endochondral bone formation includes the development of a cartilaginous model of the forming bone. MSCs first differentiate into cartilage cells (chondrocytes) and

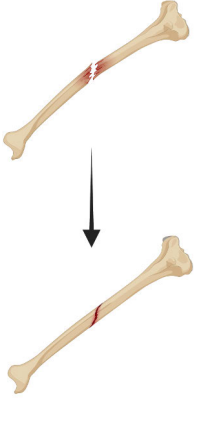
form cartilaginous model. Then, osteoblast can form a bone callus around of this structure and gradually the cartilage cells die via apoptosis and disappear via osteoclastic activity with a simultaneous osteoblast activity to replace cartilage with bone. Concurrently, blood vessels are formed to the ossifying area. Most bones develop by endochondral ossification and it also occurs during longitudinal growth and fracture healing (Anna-Marja Säämänen et al., 2022; Safadi et al., 2009).

Bone grafting to repair large bone defects are needed in oncology after tumor resections and in orthopedics and traumatology when high-energy traumas or open fractures are repaired or when prosthetic or spinal surgeries are performed (Campana et al., 2014a; Schemitsch, 2017). Globally, over two million different bone grafts are annually used, which is the second most frequent tissue transplantation right after blood transfusion (Campana et al., 2014a). However, it should be remembered that a small bone defect can repair itself because of the regenerative capacity and that bone heals without scar tissue, unlike many other tissues (W. Wang & Yeung, 2017). Biologically, bone regeneration after fracture can be divided into two major groups: direct cortical bone healing and indirect spontaneous bone healing, *i.e.* primary and secondary bone healing, respectively. (Marsell & Einhorn, 2011; Sfeir et al., 2005).

Primary bone healing is rare in natural fracture healing and it can be divided into contact and gap healing. Both forms of healing require that the bone ends are anatomically corrected and also stabilized with or without compression. In direct bone healing, fracture line is directly remodeled into Haversian canals and lamellar bone, and there is no callus, fibrous tissue or cartilage formation. In gap healing, there are two stages: first bone filling and then bone remodeling. For gap healing to occur, the distance between bone ends must be less than 0.01mm. Contact healing occurs, when osteons can grow across the fracture line, *i.e.* the fragments are perpendicular to the direction of osteons. (Marsell & Einhorn, 2011; Sfeir et al., 2005).

Secondary bone healing is the most common form of bone healing, which, in contrast of primary bone healing, does not need anatomical corrections or stabilizations of fracture line. The secondary healing includes inflammatory, reparative, and remodeling phases (Table 2), where each of phases overlap with each other, leading to a continuous bone healing process. Inflammatory phase starts right after injury, when blood vessels, cells, and bone matrix are damaged. This phase is characterized by inflammation, where inflammatory cells are recruited to the site and several pro-inflammatory factors are expressed and secreted to promote angiogenesis and recruit stem cells for differentiation and tissue repair. The first phase ends about one-week post-fracture, when reparative granuloma, *i.e.* external callus is being formed. Tissue microenvironment in the inflammatory phase is acidic and hypoxic, which is optimal for the activation of polymorphonuclear leucocytes and macrophages. (Marsell & Einhorn, 2011; Sfeir et al., 2005).

Table 2. Secondary bone healing process and biological events in the fracture side. Modified from ref. (Sfeir et al., 2005; W. Wang & Yeung, 2017). Figure on table was created in Biorender.com.

	Days after injury	Phase		Main active cells
	0–5	Inflammation	External callus formation	Monocytes, polymorphonuclear cells, macrophages, neutrophils, lymphocytes, platelets, osteoclasts, undifferentiated stem cells
5–21	Reparative	Fibrocartilage callus formation	Chondrocytes, chondroblasts, osteoclasts, macrophages, fibroblasts	
		Bony callus formation	Chondrocytes, chondroblasts, macrophages, osteoblasts, osteoclasts	
21–35	Remodeling	Remodeled bone	Osteocytes	

During the next phase of secondary bone healing, *i.e.* the reparative phase, a reparative callus tissue develops. The pH of microenvironment becomes alkaline, which is optimal for callus mineralization and alkaline phosphatase activity. Secondary bone healing can involve both intramembranous (direct) and endochondral (indirect) ossification, where intramembranous ossification creates a weight-bearing hard callus via the activity of sub-periosteal osteoblasts in fracture ends. In fracture periphery, chondrogenesis occurs to first produce soft callus (cartilage and fibrous tissue), and eventually all fibrous tissue is replaced with cartilage tissue. In the end of reparative phase, soft callus is being resorbed and replaced by hard callus via endochondral ossification. Several growth factors and cytokines are known to promote the callus formation and extracellular matrix calcification, as well as to recruit stem cells and bone cells (osteoblasts and osteoclasts) to form woven bone. (Marsell & Einhorn, 2011; Sfeir et al., 2005).

In the remodeling phase, woven bone is being resorbed and replaced with lamellar bone. The remodeling phase continues until bone has similar mechanical properties and architecture as before injury. This takes years and the complete healing time depends especially on patient age but also on fracture location and bone tissue type (cortical vs. trabecular). In addition, an essential feature in bone repair is revascularization and angiogenesis. Without necessary neovascularization, the regenerating tissue will not receive enough oxygen and nutrients, which could lead

to a non-union. In addition, pseudoarthrosis or hypertrophic non-union can develop without a stable fixation of the tissue. (Marsell & Einhorn, 2011; Sfeir et al., 2005).

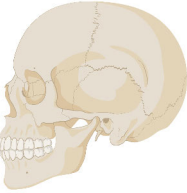
In major bone defects, where bone has been extensively lost, the defect is not able to heal via primary nor secondary bone healing process (W. Wang & Yeung, 2017). Such a defect size is the definition for a critical size and needs to be reconstructed (Schemitsch, 2017). Critical size can be definite, *i.e.* the defect cannot spontaneously heal during the lifetime, or be a defect, which is regenerated less than 10% during the lifetime (Schemitsch, 2017; W. Wang & Yeung, 2017). However, absolute and relative sizes of a defect are not the only parameters to define the critical size because of numerous other factors, such as patient age, defect's anatomical location and comorbidities affect the healing. Therefore, the definition of critical size is still widely debated, particularly when the defect size is 1–3 cm (Schemitsch, 2017).

2.1.3 Repairing the bone defects with biomaterials

Bone defect, which exceeds the critical size, needs to be repaired with bone filling or implant material. Allografts are widely used as a gold standard for bone substitute materials or alternatively autografts or xenografts can be utilized. However, these kinds of bone implant materials have several limitations, such as donor site pain, neurovascular injury or a cosmetic problem in the case of autografts, infection and disease transmission in the case of allograft and xenograft, and there are also sterilization and storage problems with xenografts. (Baldwin et al., 2019; Campana et al., 2014b; T. Kim et al., 2020; Monchau et al., 2013). However, the tissue grafts are not covered more in detail in the context of this thesis. To avoid these limitations, synthetic bone filling materials have been developed to be used as implant materials for defects caused *e.g.* by trauma, or degenerative or developmental disorders (Lieberman et al., 2005). Various synthetic biomaterials with different chemical as well as topographical properties are currently available (described in more detail in chapter 2.2). In addition to chemical and topographical properties, biomaterials' characteristics can enhance the capacity of material to integrate in bone tissue and trigger beneficial responses in bone cells. These properties are typically due to biomaterials' surface topography, surface changes or microenvironmental changes caused by the material, such as dissolved ions and/or pH changes. All biomaterials must be biocompatible to avoid negative effects, such as causing infections, toxicity or rejection reactions or having systemic adverse effects. Biocompatibility and solubility are one of the general criteria for the selection of *e.g.* ceramics to medical applications (El-Meliegy & van Noort, 2012). Other general criteria for ceramics are chemical solubility, mechanical properties, thermal behavior, refractive index and esthetic properties. The last two mainly concern biomaterials for dentistry. As an

example, clinically important properties of various cranioplasty implant materials are presented in Table 3.

Table 3. Clinically important properties of a cranioplasty implant. Modified from ref. (Vallittu, 2017). Figure on table was created in Biorender.com.



	RESORBABILITY	OSTEOCONDUCTIVITY	OSTEOINDUCTIVITY	NEOVASCULARIZATION	FLEXULAR STRENGHT OVER 600MPA	THERMAL ISOLATION	BONE-LIKE RADIOCAPACITY	MRI-COMPATIBILITY	ANTIMICROBIAL ACTIVITY	IN SITU MOLDABILITY	OVERLAY STRUCTURE
AUTOLOGOUS BONE	+/- ¹	+/- ¹	+/- ¹	+/- ¹	-	+	+	+	-	-	-
TITANIUM	-	+	-	-	+	-	-	+/-	-	+/-	+
HYDROXYAPATITE (HAP)	+	+	+	+	-	+	+	+	-	-	-
TRICALCIUMPHOSPHATE	+	+	+	+	-	+	+	+	-	-	-
POLYETHERETHERKETONE (PEEK)	-	-	-	-	-	+	-	+	-	-	+/-
POLYMETHYL-METHACRYLATE (PMMA)	-	-	-	-	-	+	-	+	-	-	-
POLYETHYLENE	-	-	-	-	-	+	-	+	-	-	+/-
BG S53P4	+	+	+	+	-	+	+	+	+	-	-
GLASS FIBER-REINFORCED COMPOSITE WITH BG S53P4 (FRC-BG)	+/- ²	+	+/- ²	+/- ²	+	+	+	+	+	-	+

1) bone integration impact properties 2) the BG + and FRC -

At the defect site, the biomaterial should optimally fill the defect and integrate into the host tissue without fibrous capsule formation. Mechanical and surface properties of a biomaterial should be optimal for material integration. Mechanical properties support tissue regeneration and optimal surface porosity and large surface area offers a route for anabolic and metabolic transfer (El-Meliegy & van Noort, 2012). In addition, surface properties promote host tissue ingrowth, as well as proliferation and differentiation of bone cells, which are described as osteopromotive and osteogenic properties, respectively (Shanmugam & Sahadevan, 2018). In the end, biomaterial integration into host tissue occurs through activation of MSCs

within the surrounding tissues to differentiate into the osteogenic cells and to allow the host tissue to grow to the biomaterial surfaces. Such phenomena are called osteoinduction and osteoconduction, respectively (El-Meliegy & van Noort, 2012; Goldberg & Akhavan, 2005; Shanmugam & Sahadevan, 2018).

Bone infection at the implantation site can be caused by bacteria that enter through a trauma, hematogenous spreading or surgical procedures (Lindfors et al., 2017). Infection causes a risk for bone necrosis, which can be avoided with a local or systemic antibiotic treatment (Lindfors et al., 2017; Wall et al., 2021). However, the use of antibiotics can cause further issues, such as development of multi-resistant bacteria or challenges in choosing the optimal dose of antibiotics (Lindfors et al., 2017; Wall et al., 2021). Biomaterials, such as bioactive glass, which possess antibacterial properties, have therefore been shown to be beneficial in the prevention and treatment of bone infections (Lindfors et al., 2017).

A biomaterial, which is capable of integrating into bone and forming a bond with it, has been described as bioactive. Specifically, the term bioactivity was defined by Larry Hench in 1996 as follows: “A bioactive material is one that elicits a specific biological response at the interface of the material which results in the formation of a bond between the tissues and the material” (Cao & Hench, 1996). In other words, this means the ability to form a hydroxyapatite layer on the bioactive glass surface, which enables the biomaterial to bind to bone tissue. The apatite formation on bioactive surfaces however begins with ion exchange within the microenvironment, thus contributing to osteogenesis (described in more detail in chapter 2.2.2.5). Therefore, the definition of the term of bioactivity has recently been critically discussed (Darvell, 2021).

In case of a biostable biomaterial, such as metal implant or ceramic implant (*e.g.*, Al₂O₃, titanium), the implant cannot bind to bone and often a fibrous capsule is formed around the implant via the foreign body reaction (Rahmati & Mozafari, 2019). Foreign body reaction consists of several incidents. After the implantation of biomaterial into the fracture site, extracellular fluid interact with its surface and plasma proteins are dynamically adsorbed and desorbed on the material surfaces, known as the Vroman Effect (Anderson et al., 2008). Topographical properties of biomaterials’ surface are important for optimal protein adsorption. The protein adsorption and blood-clotting cascade forms a temporary provisional matrix, which provides microenvironment for cell proliferation and migration (Anderson et al., 2008). Next, inflammation with the presence of different inflammatory and immune cells takes place. In the end, granulation tissue is formed by macrophages and fibroblasts, characterized by neovascularization and regenerating tissue (Anderson et al., 2008). The fibrous capsule, which has formed around the implant material can loosen and could eventually lead to implant loosening and failure (Rahmati & Mozafari, 2019). However, modifications of the implant surface, like coating

implant surface with bioactive material, can reduce this reaction of body (Rahmati & Mozafari, 2019).

2.1.3.1 Biomechanical and topographical properties of biomaterials

Biomaterials' mechanical and topographical properties are important for the implant integration into bone. Most successful implants are those, in which the mechanical properties, such as flexural and tensile strength, elastic modulus and fatigue resistance are near to bone's own mechanics. This means for instance that biomaterial with inadequate modulus of elasticity and strength cannot mechanically well enough support the tissue under healing, whereas the biomaterial of high modulus of elasticity can cause bone resorption and hinder bone formation via stress shielding (Shanmugam & Sahadevan, 2018; L. Wang et al., 2020). Before the regenerated bone tissue can be mechanically loaded, the biomaterial have to provide sufficient mechanical support to the tissue (L. Wang et al., 2020).

Body's movements cause load and stress forces, *e.g.* compression, shear and tension (Reddy et al., 2009). The ability of biomaterial to resist load deformation is described by Young's modulus of elasticity, which depicts to stress/strain of the material (Reddy et al., 2009). Biomaterials' mechanical properties define the resistance of biomaterials to different forces. For assessing implant materials in terms of mechanical properties, many biomechanical tests have been standardized with International Standard guidelines and procedures (*e.g.* ISO, ASTM, DIN, CEN) (Roeder, 2013; L. Wang et al., 2020).

2.1.3.2 Effects of ions released from biomaterials

Many inorganic ions, such as metals (Mg, Si, Sr, Zn, Cu, Co), are naturally present in the human body as part of bone mineral and have important roles in coenzymes, ion channels etc. (Hoppe et al., 2011; W. Wang & Yeung, 2017). In addition, such ions as biomaterial dissolution products have shown both bone anabolic and antibacterial effects (Hoppe et al., 2011). Common ions of biomaterials' dissolution products and their effects on bone regeneration are presented in Table 4. However, it should be noted that metals in high concentrations have toxic effects (W. Wang & Yeung, 2017).

Silicon is the second most common element in earth's crust and in nature silicon mainly occurs in oxides as silica (SiO_2) or silicates (SiO_4^{4-}) (Habibovic & Barralet, 2011; W. Wang & Yeung, 2017; Zhou et al., 2017). In living tissue, silica is present in all organisms and mainly as a component of glycosaminoglycans in the human connective tissues (Habibovic & Barralet, 2011; Zhou et al., 2017). In addition, silicon obtained via nutrition has shown positive effects on bone and

collagen production in animals (Zhou et al., 2017). Silicate ions have also been reported to have positive effects on bone homeostasis, mineral density, bone formation etc. leading to decreased bone loss (Kim et al., 2013; Uribe et al., 2020; Zhou et al., 2017), suggesting a positive effect on bone repair and regeneration. In nanoparticles, sodium silicate has been shown to inhibit osteoclasts (Mladenović et al., 2014) and stimulate the differentiation of osteoblasts (Beck et al., 2012; Uribe et al., 2020). When aiming to enhance bone remodeling and repair by biomaterials, the most familiar source of silica is from silica-based bioactive glasses (Si content <60 wt%). Dissolution of bioactive glass in the extracellular fluid forms a HAP layer, which can then make a bond with bone (described in more detail in chapter 2.2.2.5). Silica has also been used as a doped material for hydroxyapatite and tricalcium phosphate with positive results (Zhou et al., 2017). However, it has also been critically discussed if such effects are due to silicate ions or due to biomaterial's topographical changes, such as HAP formation in case of bioactive glasses (Bohner & Miron, 2019; Habibovic & Barralet, 2011).

Table 4. Effects of inorganic ions to the bone regeneration. Modified from refs. (Bose et al., 2013; Hoppe et al., 2011).

IONS	EFFECT ON BONE TISSUE
Si	Osteogenesis, angiogenesis
P	Osteogenesis
Ca	Osteogenesis
Zn	Osteogenesis
Mg	Angiogenesis
Sr	Osteogenesis, angiogenesis
Cu	Angiogenesis

2.2 Ceramics and glasses as biomaterials

Many biomaterials have been developed and studied as bone filling materials to repair and reconstruct bone. These different biomaterials can be classified into different groups either by source, into natural and synthetic biomaterials, or by their properties, into bioinert, bioresorbable and bioactive materials (Shanmugam & Sahadevan, 2018). Some bioactive materials can be bioresorbable or non-resorbable (Best et al., 2008). In this thesis, the biomaterials are divided into biostable and bioresorbable materials.

Biostable material is inert and causes minimal reactions in biological environments and host tissue. These materials are mainly metals, such as titanium, cobalt-chromium alloy and stainless steel, or ceramics, such as alumina, and zirconia. They have acceptable or good physical and mechanical properties, and biocompatibility.

Common bioresorbable materials are dissolving and interact with host tissue at the implantation side and are slowly replaced by new bone tissue (Shanmugam & Sahadevan, 2018). However, the dissolving and degrading behavior of a biomaterial should not be too quick to avoid complications with tissue replacement and new bone formation (El-Meliegy & van Noort, 2012). Different calcium phosphate compounds are a good example of bioresorbable ceramics. Bioactive biomaterials form an apatite layer on their surface and can thereby bond to bone (Shanmugam & Sahadevan, 2018). Different biostable and bioresorbable biomaterial and their properties are listed in Table 5.

Table 5. Properties of bioactive glass and ceramics, and their biomaterial applications. Modified from refs. (AlMaimouni et al., 2020; Eliaz & Metoki, 2017; Fagerlund et al., 2013; Hench & Andersson, 1993; Ishikawa, 2019; Nasar, 2019; Samavedi et al., 2013).

MATERIALS	CHEMICAL COMPOSITION	CHEMICAL PROPERTIES		CLINICAL APPLICATIONS
		Ion dissolution and degradability		
ALUMINA	Al ₂ O ₃	-		<u>Cranial and otolaryngological implants and maxillofacial reconstruction:</u> bioactive glasses, HAP, alumina, titanium <u>Dental implants:</u> alumina, zirconia, titanium, metals with HAP or bioactive glass coating. <u>Periodontal and alveolar augmentations:</u> HAP, TCP, bioactive glass <u>Bone space fillers:</u> TCP, bioactive glasses <u>Orthopedic devices (load bearing):</u> alumina, zirconia, titanium metals with HAP or bioactive glass coating.
TITANIUM	Ti	-		
ZIRCONIA	ZrO ₃	-		
TRICALCIUM PHOSPHATES	Ca ₃ (PO ₄) ₂	+		
HYDROXYAPATITE	Ca ₁₀ (PO ₄) ₆ (OH) ₂	+/- ¹		
CARBONATED APATITE	Ca ₁₀ (PO ₄) ₆ (OH) ₂ with carbonate substituting group, type A type B	+		
BIOACTIVE GLASS 45S5	24.4wt% Na ₂ O, 24.5wt% CaO, 6wt% P ₂ O ₅ , 24.5wt% SiO ₂	+		
BIOACTIVE GLASS S53P4	23wt% Na ₂ O, 20wt% CaO, 4wt% P ₂ O ₅ , 53% SiO ₂	+		
BIOACTIVE GLASS 13-93	6wt% Na ₂ O, 20wt% CaO, 4wt% P ₂ O ₅ , 53% SiO ₂ , 12wt% K ₂ O, 5wt% MgO	+		

1) Biomaterial may dissolved during long time period.

2.2.1 Biostable materials

2.2.1.1 Alumina

Alumina (Al_2O_3) is the first clinically widely used bioceramic in orthopedic implants since 1970s (Hench, 1991; McEntire et al., 2015). Alumina has shown to be biocompatible, bioinert and corrosion resistant and have good mechanical properties (Hench, 1991). However, the fracture rate (13%) was high in clinical trials with the first alumina generation, but the development of third alumina generation has improved bending strength and microstructure, such as grain size and density (Masson, 2009; Rahmati & Mozafari, 2019). In addition, mechanical properties are improved in alumina ceramic composite, which includes zirconia (17% of volume) (Masson, 2009).

Alumina is biostable and inert, and therefore cannot bond to bone. At implantation site, alumina can provoke a foreign body reaction via an immunological response (Rahmati & Mozafari, 2019). Therefore, alumina surfaces have been improved by functionalization with *e.g.* a bioresorbable material for better integration into host tissue (see chapter 2.2.3.) (Rahmati & Mozafari, 2019).

2.2.1.2 Zirconia

Zirconia (ZrO_2) has three crystalline phases: monoclinic, cubic and tetragonal (Manicone et al., 2007) with the last having the strongest mechanical resistance (Perrichon et al., 2017). However, tetragonal phase is metastable at room temperature, but it can be stabilized by metal oxides Y_2O_3 , MgO or CaO to obtain molecular stability (Manicone et al., 2007; Perrichon et al., 2017). Partially yttria stabilized zirconia (Y-TZP) is the most commonly used zirconia ceramic, because of its relatively good mechanical properties (Manicone et al., 2007; Perrichon et al., 2017). Improved fracture toughness of Y-TZP is obtained by transformation of crystalline phase from tetragonal to monoclinic by surface cracking energy (Perrichon et al., 2017). The phase transform of zirconia includes expansion of structure, and the propagation of cracks is prevented (Perrichon et al., 2017). However, despite of toughening mechanism of Y-TZP the material is classified as a brittle material.

Y-TZP has been used in orthopedic materials for hip prostheses in the 1990s (Gopal & Manivasagam, 2018). However, implant failures occurred because of low-temperature degradation, *i.e.* aging of material in water containing environment (Gopal & Manivasagam, 2018). The phenomena were caused by zirconia's phase transformation and the penetration of water into zirconia's crystal and grain structure (Chevalier, 2006; Gopal & Manivasagam, 2018). Although zirconia has better

mechanical strength and fracture toughness than alumina in dry conditions (Perrichon et al., 2017), alumina is more commonly used in joint surfaces of orthopedic implants (Chevalier, 2006; Gopal & Manivasagam, 2018).

2.2.2 Bioresorbable materials

2.2.2.1 Tricalcium phosphates

Tricalcium phosphate ($\text{Ca}_3(\text{PO}_4)_2$, TCP) has three polymorphs α -, α' -, and β -TCP. However, the α' -TCP is only present at temperatures over 1400°C (Carrodeguas & De Aza, 2011). The α - and β -TCP have both been used in clinical applications for bone regeneration and repair. Both of the polymorphs differ from each other by their crystallographic structure and thus their solubility in water and density are different too (Carrodeguas & De Aza, 2011). The α -TCP is more reactive and soluble than β -TCP, which limits the use of α -TCP in clinical applications and therefore it is mainly used in bone cements (Eliaz & Metoki, 2017). β -TCP is osteoconductive, osteoinductive and degradable by osteoclasts and it is widely used as biodegradable bioceramics in particles or blocks in clinical applications for bone repair (Bohner, 2000; Carrodeguas & De Aza, 2011; Eliaz & Metoki, 2017).

2.2.2.2 Hydroxyapatite

Synthetic hydroxyapatite (HAP), which is commonly written out as the hexagonal unit $\text{Ca}_{10}(\text{PO}_4)_6(\text{OH})_2$, has been used in orthopedics since 1982, when it was approved for clinical use by U.S. Food and Drugs Administration (FDA) (Oonishi Jr et al., 2014). Biocompatible HAP has been used in many clinical applications as particles or in scaffolds for bone filling material, metal implant's coating material and in drug delivery (Choi et al., 2020; Eliaz & Metoki, 2017; Oonishi Jr et al., 2014).

Hydroxyapatite is most stable of the clinically used bioceramics with a low solubility in water, and slow reduction when compared to other calcium phosphates, such as tricalcium phosphates ($K_{sp} \approx 10^{-58}$ and $K_{sp} \approx 10^{-25}$ - 10^{-29} , respectively) (Samavedi et al., 2013). The mechanical properties and fracture toughness of HAP are weak but due to its good compressive strength, it can be used as coating material of implants (W. Wang & Yeung, 2017).

2.2.2.3 Carbonated apatite

Carbonated apatite (CAP) differs from hydroxyapatite, $\text{Ca}_{10}(\text{PO}_4)_6(\text{OH})_2$, by carbonate's substituting groups. Carbonate can be substituted by OH^- (type A) or

PO_4^{3-} (type B). Carbonate's substituting groups and degree of carbonation affects carbonated apatite's solubility and crystallinity (Madupalli et al., 2017). CAP has also been reported to be more osteoinductive than sintered HAP. In addition, osteoclasts can resorb CAP, but not HAP, which makes CAP more resorbable and thus a better bone repair can be expected to occur at the implantation site (Ishikawa, 2019). Carbonated apatite has been accepted to be used as an augmentation material of dental implants by the Japanese Pharmaceutical and Medical Device Agency (PMDA) in 2017 (Ishikawa, 2019).

2.2.2.4 Calcium carbonate

Calcium carbonate (CaCO_3 , CC) with its crystalline anhydrous forms of calcite and aragonite is stable and metastable, respectively, and can be used as a bone filling material. CC for biomaterial applications often originates from natural corals (Ben-Nissan, 2003; Monchau et al., 2013). It is biocompatible, osteoconductive and a highly resorbable biomaterial via osteoclast activity (Demers et al., 2002). It has been widely investigated as a bone filling material of natural origin from corals since 1970s, and has been used in orthopedic surgery (Ben-Nissan, 2003; Demers et al., 2002). However, corals as xenografts have several limitations in medical use and ecological and natural conservation reasons have limited its wider use in surgery. Hence, to avoid the limitations of natural CC, synthetic CCs have been also developed and studied (Chróścicka et al., 2016; Monchau et al., 2013).

2.2.2.5 Bioactive glasses

In the 1970s Larry Hench and coworkers at the University of Florida developed first silica-based glasses with an intention of developing a material, which can chemically bind to the host tissue (Hench, 1991). They were successful in their development with an amorphous glass composition $\text{Na}_2\text{O-CaO-P}_2\text{O}_5\text{-SiO}_2$ close to a ternary eutectic in diagram of $\text{Na}_2\text{O-CaO-SiO}_2$, which was named BG 45S5 with a composition of 24.4wt% Na_2O , 24.5wt% CaO , 6wt% P_2O_5 and 24.5wt% SiO_2 (Jones et al., 2016). The composition of this glass includes only the components of natural bone mineral HAP (calcium and phosphorus) and some other ions (sodium and silicon), which are naturally abundantly present in human body (Hupa, 2018).

Modification of bioactive glasses and research on their potential applications led to S53P4 development in Turku, Finland in the 1980s. BG S53P4 is silicate glass like 45S5 and these bioactive glasses differ only slightly from each other (BG S53P4: 23wt% Na_2O , 20wt% CaO , 4wt% P_2O_5 , 53% SiO_2). To improve the physical properties of BGs 45S5 and S53P4, K_2O and MgO were doped into these bioactive glasses and thereafter bioactive glass 13-93 (6% Na_2O , 12wt% K_2O , 5wt% MgO ,

20wt% CaO, 4% P₂O₅, 53% SiO₂) was developed (Fagerlund & Hupa, 2017; Hupa, 2018). These three bioactive glasses 45S5, S53P4 and 13-93 are the only, which are approved for clinical use in Europe and also in the U.S. (Fagerlund & Hupa, 2017; Hupa, 2018; Vallittu, 2017).

The amorphous bioactive glasses 45S5 and S53P4 do not form symmetry arrangement or long-range order of atoms. However, SiO₄ tetrahedron forms short-range orders, where oxygen forms zero to four bridges to other SiO₄ (Brauer & Möncke, 2017). Usually, one SiO₄ has low bridging and Si-OH groups exist, which enables the bioactive properties, such as ion dissolution and HAP layer formation on bioactive glass surface. In addition, other molecules such as Na₂O also influence the numbers of bridges to oxygen (Hupa, 2018).

Manufacturing methods influence the physicochemical properties of bioactive glasses. Bioactive glass can be formed by a sol-gel or melt-derived methods. The methods influence numbers of Si-OH groups, glass degradability and bioactivity (Brauer & Möncke, 2017). The sol-gel derived glasses are more degradable and bioactive than melt-derived because of greater numbers of Si-OH groups (Brauer & Möncke, 2017).

BG's affinity to bond to bone is due to the surface bioactivity by leaching ions and in the end forming a hydroxyapatite layer. Ions start to dissolve into the microenvironment subsequently when the BG becomes into a contact with the extracellular liquid of the tissue (Vallittu et al., 2015). BG's surfaces reactions are divided into the 12 steps defined by L. Hench, starting from the five reactions of ion dissolution up to the last seven reactions of bone formation by bone cells (Hench, 1991) (Table 6). It however needs to be emphasized that BGs' surface reactions depend on both the composition of surrounding fluids and the chemical composition of BG (Nommeots-Nomm et al., 2020).

Table 6. Twelve steps of bioactive glasses' surface reactions to form bond with bone. Modified from ref. (Hench, 1991).

0	Bioactive glass surfaces
1	Ion changes between biomaterial and body solution, Na ⁺ or K ⁺ with H ⁺ or H ₃ O ⁺ , respectively. Si-O-Na⁺ + H⁺ + OH⁻ → Si-OH⁺ + Na⁺ + OH⁻
2	Soluble silica (SiO ₂) loss and formation of silanols (Si-OH) at the bioactive glass surface. Si-O-Si + H₂O → Si-OH + OH-Si
3	Silanols condensation and repolymerization. SiOH + SiOH → Si-O-Si + H₂O
4	Adsorption of Ca ²⁺ and PO ₄ ³⁻ ions on the SiO ₂ layer by forming amorphous CaO-P ₂ O ₅ layer.
5	Amorphous CaO-P ₂ O ₅ layer will crystallize via ion exchange and in the end form hydroxyl carbonate apatite (HCA).
6	Biological moieties are adsorbed in HCA-layer
7	Primary infections cells arrive to surfaces of bioactive glasses <i>i.e.</i> macrophages
8	Stem cells attach to the changed surface of bioactive glass
9	Stem cells differentiate
10	Matrix is generated
11	Matrix is crystallized
12	Bone tissue – cell proliferation and growth

Interface reactions happen in the first five steps, which start by ion exchange between BG's alkaline ions and interfacial fluid's hydroxyl ions, which allows the pH in the microenvironment to rise and silica groups to be hydrolyzed (Hench, 1991; Hupa, 2018). In the next stages, a silica rich layer is formed at the BG interface via condensation and repolymerization. In this large surface and water-containing silica-rich layer, the calcium and phosphorus are adsorbed and an amorphous calcium phosphate layer is forming. Then, hydroxyl and calcium dioxide ions are incorporated into calcium phosphate layer and hydroxyapatite layer forms *in vitro* by a solid-state transformation (Hench, 1991; Vallittu, 2017).

Formed HAP or CAP layers are optimal for cell adhesion, proliferation and differentiation, *i.e.* the surfaces are osteoconductive (Hench, 2009). The last seven Hench's steps describe these biological reactions. First, the biochemical growth factors are adsorbed into the hydroxyapatite layer, which is followed by macrophage action and then stem cell proliferation and differentiation.

BGs' interfacial reaction, where ions are exchanged with surrounding fluids, has also a major clinical importance. The exchange of ions and elevated pH value with a changed osmolarity in the microenvironment gives antimicrobial properties for BGs (Vallittu, 2017). The pH and osmolarity causes a pressure difference between the bacterial cell membrane and surrounding fluids, which causes disruption of cell membrane and thereby impairs bacterial viability (Lindfors et al., 2017). However, BGs' composition, surface area, manufacturing methods, and fluid circulation *in vivo*, all influence the antimicrobial outcomes (Lindfors et al., 2017). For example, even though BG 45S5 has the same basic chemical element contents than BG S53P4, it can show a higher increase in pH and more effective antimicrobial impact. However, when the effects of BG to osteogenic cells are considered, BG S53P4 has a better balance between the antimicrobial properties and osteogenic potential (Vallittu, 2017).

BGs antimicrobial properties are clinically important due to the clinical need to treat bone and periprosthetic infections. Several clinical studies have shown that BG S53P4 has beneficial effects against chronic osteomyelitis without using antibiotics (Lindfors et al., 2017). This is a major benefit of BGs, because the extensive use of antibiotics needs to be reduced to prevent the development of antibiotic resistant microbial strains (Lindfors et al., 2017). BG S53P4 has been shown to be efficient against many clinically relevant bacteria, and even multi-resistant strains *in vitro* and *in vivo* (Lindfors et al., 2017). In addition, both bioactive glasses 45S5 and S53P4 have shown osteoinductive, osteoconductive and pro-angiogenic properties both *in vitro* and *in vivo* (Hench, 2009; Vallittu et al., 2020).

2.2.3 Surface-modified materials

Material surface properties influence the interactions with proteins and cells, as previously described (see chapter 2.1.3.1). Surface properties of many clinically used implant materials have been improved by different surface modifications in order to affect the interactions of proteins and cells with biomaterial surfaces. For example, alumina surfaces have been modified with bioactive materials, such as bioactive glass or HAP (Rahmati & Mozafari, 2019).

Alumina is a widely used biomaterial in orthopedics and its surface properties have been modified by coating or functionalization (Camilo et al., 2017; Rahmati & Mozafari, 2019). For instance, functionalization with bioactive glass (BG 45S5) has shown promising results (Camilo et al., 2017). Bioactive glasses' major component is silica, which has pro-angiogenic and osteogenic properties (Bose et al., 2013) (see chapter 2.1.3.2) and silica-modified alumina particles have also been used in dentistry to improve the technical adhesion of resin-based materials to ceramic or metal substrates. The method where silica-modified alumina particles were used is a

tribochemical silica-coating method (TSC) (Khan et al., 2019; Matinlinna & Lassila, 2004; Özcan & Vallittu, 2003). Interestingly, the potential of silica-modified alumina particles in the context of bone filling material applications has not been studied before this thesis.

Functionalization has also been used for bioresorbable materials. For example, low resorbing HAP has been used as a coating of fast resorbable CC (Fu et al., 2013; Walsh et al., 2003). Material modifications of this kind have been studied *in vivo* and showed to improve bone formation and mineralization (CHACC, ProOsteon) (Fu et al., 2013; Jamali et al., 2002; Ong et al., 2012; Ripamonti et al., 2009). One new functionalized calcium carbonate (FCC) consists of HAP surface and CC core, and the HAP content can vary 13–85% in different products (Roth, 2019). It has been originally developed for and studied in industrial applications, *e.g.* pharmaceutical industry and agriculture (Levy et al., 2017; Roth, 2019). Similar to silica-modified alumina, FCC includes two biomaterials, which have been separately studied as bone filling material applications but not as combined multimaterials.

2.3 In vitro characterization of biomaterials

Biomaterials have to be biocompatible and fill the requirements for a safe implantation into tissues. Biomaterials affect differently the microenvironment at implantation sites. Bioresorbable and bioactive materials leach different ions, which influence ion concentrations, osmolarity and pH in the microenvironment. These and other properties have biological impact on the activation of osteogenic cells towards bone formation and greatly depend on bioceramics' chemical composition. Thus, it is important to characterize biomaterials both physicochemically and biologically, before proceeding into preclinical and clinical studies.

2.3.1 Physicochemical and surface characterization

Biomaterial properties, such as chemical structure, composition, surface properties and ion dissolution are essential for understanding the differences of different materials. These properties of materials also influence the biological environment, such as cell and tissue microenvironments and their interactions with biomaterials.

Material physical and chemical properties can be characterized with several methods, which are summarized in Table 7. However, many methods, which are used to assess a certain material property, can give variable results, as the quality and sensitivity of analysis varies between different methods. Therefore, it is important to know the different characterizations methods well and to use the best methods for the properties of interest.

Attenuated Total Reflectance Fourier Transform Infrared (ATR-FTIR) can be used to characterize biomaterials physicochemical properties, such as vibrational features of material compounds. The method is based on natural vibrations of materials chemical bonds, when the materials absorb infrared (IR) radiation. The material adsorbs IR-radiation only, when there is resonance with materials' natural molecular vibration. To simultaneously detect all transmitted energy interferometer and Fourier transform algorithm (FT) is used. Attenuated total reflectance (ATR) is used for opaque and solid samples and it is also nondestructive. In ATR method, the IR-radiation goes through the materials and reflects from the surfaces of the materials. (Sampath Kumar, 2013)

Biomaterials phase composition, crystalline size and crystallographic orientation can be characterized by X-Ray power Diffraction (XRD) and biomaterial's morphology and elements can be characterized by Scanning Electron Microscopy-Energy-Dispersive X-ray Analysis (SEM-EDXA). The XRD is based on monochromatic and atomic scale X-ray diffraction on the material. The intensity of diffracted X-ray is measured as a function of diffracted angle, and thus the atomic planes of the material can be calculated by Bragg's law. (Sampath Kumar, 2013)

In SEM technique, the material surfaces are scanned with a focused electron beam. The electron beam interactions with atoms of material surfaces are emitted as various signals. The intensity of signals is detected in detectors, where the intensity of emitted signals is converted to an image. The elemental analysis or chemical characterization can be performed with SEM equipped with EDX. EDX measures the quantity and energy of emitted X-rays of the material. An emitted X-ray is typical from the atomic structure of element, and thus materials' elements can be characterized. (Sampath Kumar, 2013).

Biomaterial ions' dissolution in different fluids can be studied with comparable methods, such as in a static environment or in continuous flow-through. The fluid flow is known to vary in different parts and tissues of human body, *i.e.* the physiological fluid flow is not static. For this reason, continuous flow-through methods have been developed according to a variety of physiological fluid flow. However, static dissolution is also a good method, for example for minor quantities of dissolved ions, indicating that the selection of dissolution system must be based on the studied property of materials. Dissolved ions in fluids can be analyzed by Inductively Coupled Plasma Optical Emission Spectrometry (ICP-OES) and the possible surface modifications with FTIR, SEM and XRD. (Fagerlund & Hupa, 2017; Hupa, 2018; Maçon et al., 2015).

Table 7. Common physicochemical characterization methods of biomaterials.

PROPERTIES OF BIOMATERIAL	METHODS OF CHARACTERIZATION
PHYSICAL AND CHEMICAL	Optical/electron microscopy, CA, SEM, XRD, FTIR, DLS, Mercury intrusion, gas adsorption
SURFACE	XPS, AES, SIMS, Surface-MALDI-MS, IR, Raman spectroscopy, EELS, UV-vis, light/confocal microscopy, SEM, TEM, STM, AFM, Profilometry, CA, ellipsometry
BIOACTIVITY AND ION DISSOLUTION	Continuously dissolution, Static dissolution, ICP-OES

Table contents compiled from refs. (Fagerlund et al., 2012; Maçon et al., 2015; Sampath Kumar, 2013; H. Wang & Chu, 2013; Wong, 2021)

2.3.2 Biological characterization

After the biomaterial has been characterized for its physicochemical properties, the next step is to carefully evaluate it biologically to assess its biocompatibility *in vitro*. If biomaterial shows biocompatibility and a potential to be used as a bone filling material, it can be further investigated by preclinical *in vivo* studies. However, the biological *in vitro* studies consist of many different studies of cells biocompatibility and interactions with biomaterials (Table 8). Taking into account that the bone repair involves many different cell types (as described earlier in chapter 2.1.2), the biomaterial has to show biocompatibility for all cell types (e.g. osteoblasts, osteoclasts and endothelial cells), which have to studied separately *in vitro*.

The most typical method to study biocompatibility of biomaterials is to evaluate cell viability and proliferation in the presence of biomaterials or their dissolution products. The cell culture system can thus be a direct or non-direct contact between cells and biomaterial or cells cultured in the presence of biomaterial conditioned-media (Figure 1.). In the non-direct methods, the biomaterial is first incubated in cell culture medium at 37°C for 24–72 h and the extracted medium is used in cell culture. This method based on International Organization for Standardization for Medical Devices (ISO 10993). Direct methods, where cells are cultured on top of biomaterials enable cells to directly and closely interact with biomaterials. (Wong, 2021).

Table 8. Common biological characterization methods of biocompatibility.

CHARACTERIZATION OF BIOCOMPATIBILITY	Cell viability and proliferation (e.g. <i>MTT</i> , <i>MTS</i> , <i>XTT</i> , <i>WST</i>) Morphological assays (e.g. Optical microscopy, SEM, TEM, confocal microscopy, immunohistochemistry) Stem cell differentiation Cell functional assays (e.g. <i>inflammatory markers and apoptosis assay</i>) Hemocompatibility assays Genotoxicity assays Gene expression (PCR)
---	--

Table contents compiled from refs. (Omidi et al., 2017; Thasneem & Sharma, 2013; Wong, 2021)

The most commonly used methods to analyze cell viability and proliferation are different kinds of colorimetric or fluorometric assays (e.g. WST, MTT), which are based on the detection of mitochondrial ATP production or mitochondrial enzyme activity in cells. Level of ATP is high in living cells but is decreased rapidly when a cell dies. Thus, the level of ATP correlates with the number of living cells. WST and MTT assays are based on cellular mitochondria dehydrogenase enzyme, which cleaves tetrazolium salts to formazan. The dehydrogenase activity and thus the amount of formazan dye is higher in living cells and lower in dead cells and can be measured with spectrophotometer. The detected signal must be compared to the standard curve to obtain the number of living cells. (Wong, 2021).

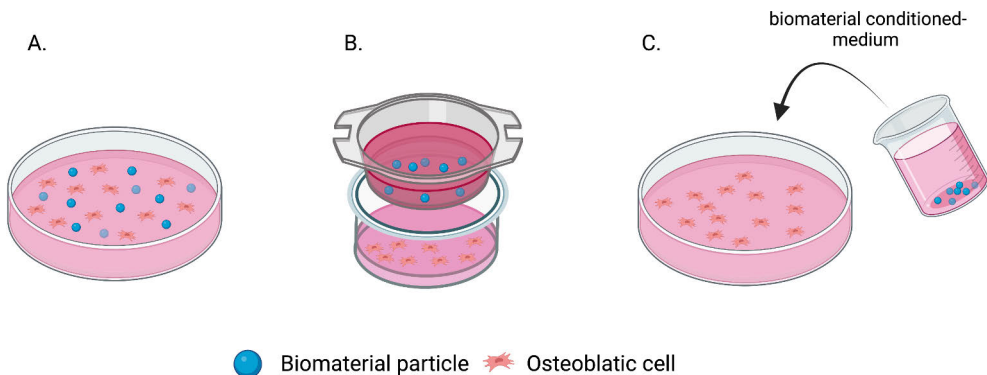


Figure 1. Cell culture methods to study for e.g. osteoblastic cell responses to biomaterials, **a.** cells and biomaterial in a direct contact, **b.** cells and biomaterial in a non-direct contact, **c.** cells cultured with biomaterial-conditioned medium. Modified from ref. (Hoppe et al., 2011). Created in Biorender.com.

3 Aims

Research methods, which are used to study biomaterials' properties, can differ between different studies and in different experimental settings. This complicates the comparison between results and their interpretation. Therefore, the aim of the thesis was to comparatively characterize different biomaterials and their combinations. Both physicochemical and biological characterization methods were applied to evaluate biomaterials' potential as bone filling materials in the future.

The specific aims of the study are listed below.

1. To compare the physicochemical properties of five clinically commonly used bioceramics, *i.e.* hydroxyapatite, carbonate apatite, bioactive glasses 45S5 and S53P4, and alumina *in vitro*.
2. To physicochemically characterize silica-modified alumina particles and compare its biological properties to the inert counterpart alumina.
3. To characterize the physicochemical and biological properties of functionalized calcium carbonate in the context of bone tissue repair.

4 Materials and Methods

4.1 Biomaterials and reagents

Different biomaterials, *i.e.* bioactive, bioresorbable and bioinert material, were studied in the context of bone repair. All materials were commercial and are listed in Table 9. Part of studied materials are commonly used and have been previously clinically studied as bone filling material (I), while parts of materials were studied for the first time in the context of bone repair in this thesis (II-III). The biomaterial particle was used for characterizing analyses because the methods were more feasible for the particle. Biomaterial particle size was selected in the comparable analyses by same order of magnitude, except HAP particle, due to availability. The two new biomaterial particles in the field of bone repair were smaller size than others because of the manufacturer.

Biomaterials, which are clinically commonly used (I) were compared by their physicochemical properties *in vitro*. Biomaterials, which were studied as bone filling material for the first time (II-III), were studied for their physicochemical properties and biological properties *in vitro*. For all cell culture studies (II-III), the biomaterials were first weighed out on alumina foil and then sterilized in the autoclave (121°C, 20 min).

In the dissolution test, Tris buffer (2-amino-2-hydroxymethyl-propane-1,3-diol, Sigma Trizma® base), α MEM (M8042 Sigma Aldrich (II) or α -MEM, Gibco, 41061 (III)) or simulated body fluid (SBF) was used. The reagents of SBF are listed in Table 10. 50mM Tris buffer was prepared by weighing out 6.057g of Trizma® base in 1 L water and then the pH value was set to 7.3 by 1M HCl.

The cell culture medium included amino acids, vitamins, ribonucleosides, deoxyribonucleosides, inorganic salts CaCl₂ (0.2g/L), MgSO₄ (0.09767g/L), KCl (0.4g/L), NaHCO₃ (2.2g/L), NaCl (6.8g/L), and also d-glucose and sodium pyruvate. In addition, the M8042 included phenol red and Na₂HPO₄ (anhydrous, 0.122g/L) and the 41061 included lipoic acids and NaH₂PO₄-H₂O (0.14g/L).

Table 9. Biomaterials used in this thesis and as specified by the manufacturers.

Original publication	Biomaterial	Particle size (μm)	Abbreviation	Composition (wt%) / Chemical structure	Manufacturer
I	Bioactive glass 45S5	500-800	BG 45S5	24.5% Na ₂ O, 45% SiO ₂ , 6% P ₂ O ₅ , 24.5%CaO.	MO-SCI Health Care, L.L.C. 4040 HyPoint North, Rolla MO 65401 USA
I	Bioactive glass S53P4	500-800	BG S53P4	23% Na ₂ O, 53% SiO ₂ , 4% P ₂ O ₅ , 20%CaO.	MO-SCI Health Care L.L.C. 4040 HyPoint North, Rolla MO 65401 USA
I	Hydroxyapatite	100-300	HAP	Ca ₁₀ (PO ₄) ₆ (OH) ₂	Berkeley advanced biomaterials, INC. 901 Grayson Street, Suite 101, Berkeley, CA 94710
I	Carbonated apatite	300-600	CAP	Ca ₁₀ (PO ₄) ₆ (OH) ₂ and two different way of carbonate substituting group. In type A carbonate is substituting for OH ⁻ and type B for PO ₄ ³⁻	Cytrans Granules GC Corporation, Tokyo, Japan
I, II	Alumina	500, 28-31	Al ₂ O ₃	99.75% Al ₂ O ₃ , 0.25% Na ₂ O, 0.02% SiO ₂ , 0.02% Fe ₂ O ₃ .	Duralum White (Washington mills USA)
II	Silica-modified alumina	30	-	> 95% Al ₂ O ₃ , 1-5% SiO ₂ , < 0.5% Na ₂ O	Rocatec Soft, 3M Espe, Germany
III	Functionalized calcium carbonate	7	FCC	51% HAP, 49% CC	Omya International AG, Switzerland

Table 10. The composition of simulated body fluid (SBF).

REAGENT	NaCl	NaHCO ₃	KCl	K ₂ HPO ₄ 3 H ₂ O	1M HCL	MgCl ₂ 6 H ₂ O	CaCl ₂ 2 H ₂ O	Na ₂ SO ₄	TRIS
AMOUNT OF REAGENT PER 2 LITRES	16 g	0.70 g	0.45 g	0.46 g	70 ml	0.61 g	0.74 g	0.14 g	12.11 g

4.2 Physicochemical characterization

4.2.1 ATR-FTIR analysis (I–III)

ATR-FTIR was used to analyze the vibrational features of biomaterial components. Biomaterials were analyzed by using a PerkinElmer Spectrum (Version 10.4.2) spectrometer. The ATR-FTIR instrument were averaged from 16 scans collected for wavenumbers from 550 or 650 cm⁻¹ to 2 500 or 4 000 cm⁻¹ at 4 cm⁻¹ resolution. The software was CPU32 Main 00.09.9934 22-4-2011 and a UATR crystal combination diamond/ZnSe at triplicate of bounces was used.

4.2.2 XRD analysis (I–III)

X-ray powder diffraction (XRD) was used to characterize the phase composition of the particles. The particles were characterized with a Bruker D8 Discover instrument (Bruker) with Cu K α radiation ($\lambda = 1.54 \text{ \AA}$). The samples were measured in the 2-theta range 5°–80°, using an increment of 0.04° and data collection of 0.2 seconds per step.

4.2.3 SEM-EDX analysis (I–III)

Scanning electron micrographic (SEM) images were taken to observe the morphology of the biomaterials (I–III) and to confirm their particle sizes (I). The SEM used was a Leo Gemini 1530 (Carl Zeiss, Oberkochen, Germany) instrument and the electron beam was accelerated with voltages of 15 or 20 kV.

Particle size was analysed by ImageJ® (1.52a) bundled with Java 1.8.0_112 (64-bit) (Wayne Rasband National Institutes of Health, USA) software by setting a scale and drawing straight lines. Two to six particles were measured by four measurements, and mean particle sized was calculated using Excel (version 1808, 10730.20334). Thickness of the reaction layer of BGs after being immersed in Tris buffer for 4 hours and 24 hours was measured from SEM images with a

magnification of 500 \times . Six measurements were made, and mean values were calculated.

Biomaterial surfaces were investigated with SEM before and after dissolution tests (I–III). Biomaterial particles, BG 45S5, BG S53P4, HAP, CAP, alumina (I), surface and surface reaction layer were characterized after a continuous dynamic dissolution test in Tris buffer after 0h, 4h, and 24h. The particles were prepared for the SEM analysis as follows: washed with ethanol, cast in epoxy resin and then cut and polished to reveal the particle cross-sections. The thickness of the reaction layers at the particle's surfaces was determined from the images taken with SEM. The oxide composition of the reaction layers that could be detected in the SEM image was analyzed using Electron Dispersive X-ray Analysis (EDXA).

Silica-modified alumina particles' (II) surface structure was investigated with SEM-EDX before and after static dissolution tests in Tris-buffered and SBF solutions (4h and 24h). For SEM examination, the particles were washed with ethanol and cast in epoxy resin. FCC particles (III) were investigated with SEM for their surface structure before and after a 14-day dissolution in the cell culture medium. After dissolution in the cell culture medium, the particles were washed with 70% ethanol before imaging.

4.2.4 pH change and ion release (I–III)

pH change and ion release were measured for all studied biomaterials (I–III) in various *in vitro* systems. Some of the materials were examined with similar tests and some were subjected to various additional tests. All studies for each biomaterial are summarized in Table 11.

4.2.4.1 pH changes and ion release in continuous dynamic system in vitro (I–III)

All biomaterials were studied in a continuous dynamic system. The release of ions was measured in a dynamic system in which a fresh solution of Tris buffer (2-amino-2-hydroxymethyl-propane-1,3-diol) was fed continuously (0.2 ml/min input) through a bed of the sample particles at 40°C. The continuous flow output was not really changed compared to the input volume. The pH of the (50 mM) Tris buffered solution (Trizma base, Sigma-Aldrich, pK_a 8.06) was regulated to 7.3 with 1 M HCl (J-T. Baker). All sample cells (diameter 5 mm, length 12 mm) were filled with materials (0.19–0.3 g; except for FCC 59 mg, because of the volume of chambers) as described previously (Fagerlund et al., 2012). The ion concentrations and pH were measured for solution samples (4 ml) collected at the time points of 20, 40, 60, 80, 100, 120, 240, 480, and 1440 min. pH was measured with Mettler Toledo, Seven Easy

electrode. For the ion analysis, 1 ml of the solution was diluted with ultrapure water (1:10) and acidified with concentrated HNO₃. The ion concentrations in the solutions were measured with Inductively Coupled Plasma Optical Emission Spectrometry (ICP-OES, PerkinElmer Optima 5300 DV, Waltham, MA, USA). The released ions were examined for silicon (LOQ 0.04 ppm, 251.611 nm), sodium (LOQ 0.2 ppm, 589.593 nm), calcium (LOQ 0.7 ppm, 393.366 nm), phosphorus (LOQ 0.03 ppm, 213.617 nm) and aluminium (LOQ 0.01 ppm, 396.153 nm).

Table 11. Measured properties of the biomaterials, which were studied in continuous and/or static in vitro systems.

		Biomaterial							
In vitro system	Measured properties	Bioactive glass 45S5	Bioactive glass S53P4	Hydroxyapatite	Carbonated apatite	Alumina	Silica-modified alumina	Functionalized calcium carbonate	
Continuous dynamic in vitro system with Tris buffer	pH value	✓	✓	✓	✓	✓	✓	✓	
	silicon, sodium, calcium, phosphorus, aluminium ions	✓	✓	✓				✓	
Static in vitro system with	pH value						✓		
	silicon ions						✓		
	silicon ions						✓		
cell culture medium	calcium ions							✓	

4.2.4.2 pH change and ion release in static in vitro system with SBF, Tris buffer and α MEM (II)

Because of silica-modified alumina particles' low amount of silica, its pH change and ion release were also measured in the static system. This was performed by incubating silica-modified alumina particles (~75 g) in 50 ml of Tris buffer or SBF in an incubator at 40°C (Orbital incubator, SI500, Stuart) with a rotation at 100 rpm (Maçon et al., 2015). The pH was measured at the same time points as in the dynamic system (20, 40, 60, 80, 100, 120, 240, 480, and 1440 min) with a Mettler Toledo Seven-Easy electrode. For the ion analysis, 1 ml of the solution was diluted with ultrapure water (1:10) and acidified with concentrated HNO₃. The ion concentrations in the solutions were measured with inductively coupled plasma optical emission spectrometry (ICP-OES, PerkinElmer Optima 5300 DV, Waltham, MA, USA). The released ions were examined for silicon (LOQ 0.04 ppm, 251.61 nm), sodium (LOQ 0.2 ppm, 589.592 nm), calcium (LOQ 0.7 ppm, 393.366 nm), phosphorus (LOQ 0.03 ppm, 213.617 nm) and aluminium (LOQ 0.01 ppm, 396.153 nm).

Silica-modified alumina's release of silica was also characterized in cell culture medium (α -MEM) to simulate silica's release in a biological environment. This was measured by a colorimetric method. The different analysing methods in silica release were used because the research work had been carried out in collaboration of two laboratories. Thus, the cell culture analysis and sample were prepared and analysed in a different place than other ion release analysis, which is why the silica release was analysed with the colorimetric methods. Silica-modified alumina particles were immersed in α -MEM (without penicillin or fetal bovine serum (FBS) in five different concentrations (0, 0.3125, 0.625, 1.25, 2.5, 5 mg/ml) and incubated at 37°C, 5% CO₂. The samples were collected at 1, 3, 7 and 10 days. The samples were centrifuged (10 G, 5 min) and supernatant was collected into new test tubes and stored in the fridge (4°C) until the colorimetric analysis. Si concentrations were analyzed by the molybdenum blue method (Ballo et al., 2008) using dilutions of a Si standard ((NH₄)₂SiF₆ in H₂O, Certipur) in five concentrations (0, 0.1, 0.3, 0.5, 0.7, 1 mg/L). Samples were diluted (1:4) with ultra-pure water. Samples and standards were mixed with antimony phosphomolybdate complex, reduced with ascorbic acid, and finally, the silicomolybdate complex was adjusted by mixing 1-amino-2-naphthol-4-sulphonic acid, sulphate and tartaric acid. Absorbances at 820 nm were measured by a UV-1601 spectrophotometer (Shimadzu, Australia).

4.2.4.3 pH changes and ion release (III)

pH change and calcium ion release of FCC was measured in a static system mimicking the cell culture system. Since calcium is the main ion type to be dissolved from FCC and the phosphorus dissolved only slightly in a continuous system, only

calcium release was measured in a static dissolution system. *In vitro* release of calcium and change in pH were measured in the static system either in cell culture medium or in ultrapure water at 37°C in a humidified atmosphere containing 5% CO₂. The pH was measured with SDR SensorDish Reader (PreSense) with HD24 and software version SDR_v4.0.0. The measuring interval was adjusted to every 15 minutes. The pH was measured with five different concentrations of FCC, *i.e.* 12.5, 25, 50, 100 and 200 µg/ml and a blank control (0 µg/ml) in cell culture medium or in ultrapure water up to 14 days. During the 14-day dissolution test, cell culture medium or water was changed every 3–4 days by carefully pipetting just below the liquid surface and avoiding touching the bottom of the wells, similar to when changing the culture medium for cells in the viability test. In another plate, cell culture medium or water was kept unchanged for the entire 14 days of dissolution. For each well, a sample for the calcium analysis was collected after 14 days of dissolution.

All calcium samples were pipetted from just below the liquid surfaces and then quickly spun. Before calcium analysis, samples from cell culture medium were diluted 1:20 and samples from water 1:10 with ultrapure water. Liquid was further mixed with 5% La-solution, centrifuged at 2800 rpm for 10 min and calcium concentrations were then measured with Atomic Absorption Spectroscopy (AAS) (PerkinElmer AAnalyst 400, with Ca-lamp).

4.3 Biological characterization

4.3.1 Cell cultures (II–III)

A mouse cell line MC3T3-E1, subclone 4, (ATCC, CRL2593) was cultured in Minimum Essential Medium Eagle (M8042, Sigma Aldrich) (II), and in phenol-red free Minimum Essential Medium (α -MEM, Gibco, 41061) (III), with 10% FBS (Gibco, 10270-106) and 1% penicillin at 37°C in a humidified atmosphere containing 5% CO₂. At sub-confluency, the cells were trypsinized and plated on 96-well plates for viability assays. All experiments were performed with cells below passage 20 and cell culture medium was changed every 3–4 days.

4.3.2 MC3T3-E1 cell viability with biomaterials (II–III)

The biological properties were studied for those biomaterials (silica-modified alumina and FCC), which were studied as bone filling material for the first time. To assess the viability of pre-osteoblasts cell in the presence of biomaterial particles, MC3T3-E1 cells were seeded at 5 000 cells/well in 96-well plates. The total volume of each well was 200 µl. Particles were sterilized and materials were suspended in

cell culture medium right before the viability experiment was started. The viability test was repeated three times in both studies (II, III).

For cell cultures with silica-modified alumina (II), the cells were let to adhere for one day before the medium was changed into the medium containing different concentrations of silica-modified alumina or alumina particles. Five different quantities, *i.e.* 0.3125, 0.625, 1.25, 2.5, 5 mg/ml of silica-modified alumina and control material alumina were used, and in both case a control of 0 mg/ml was included. Cell viability at 1, 3, 7 and 10 days was determined by a WST method (Cell Counting Kit-8, CK04, Dojindo, 1:10 dilution) by measuring the absorbance at 450 nm (Thermo Scientific, Multiscan FC with SkanIt software for microplate readers, UI version 4.1.0.43). The background absorbance without any cells (only materials at each quantity in cell culture medium) was also measured and subtracted from sample values, when viability results were analyzed.

For cell cultures with FCC (II) five different concentrations, *i.e.* FCC 12.5, 25, 50, 100 and 200 µg/ml were used, and a control (0 µg/ml) was included. Cell viability was determined as above, except one day cell adhering before biomaterial particle application into well was not done.

4.3.3 SEM and TEM imaging of MC3T3-E1 cells (III)

Scanning electron microscopy (SEM) and Transmission electron microscopy (TEM) imaging was used to analyse the localization of FCC particles within and near the cells. For SEM and TEM imaging, MC3T3-E1 cells were cultured in the presence of 12.5 µg/ml and 25 µg/ml of FCC particles on glass coverslips for 10 days. The medium was changed every 3–4 days.

For the SEM images, the samples were fixed in 5% glutaraldehyde in 0.16 M s-collidin buffer, pH 7.4, post-fixed by using 1% OsO₄ containing 1.5% potassium ferrocyanide and dehydrated with a series of increasing ethanol concentrations (30%, 50%, 70%, 80%, 90%, 96%, and twice 100%). The samples were then immersed in hexamethyldisilazane and left to dry by solvent evaporation. The samples were examined using a Leo Gemini 1530 (Carl Zeiss, Oberkochen, Germany) instrument operated at 2.7 kV acceleration voltages.

For TEM images, the samples were fixed with 5% glutaraldehyde in s-collidine buffer, post-fixed with 1% OsO₄ containing 1.5% potassium ferrocyanide, dehydrated with ethanol, and embedded in 45359 Fluka Epoxy Embedding Medium kit. Thin sections were cut using an ultramicrotome to a thickness of 70 nm. The sections were stained using uranyl acetate and lead citrate. The sections were examined using a JEOL JEM-1400 Plus transmission electron microscope operated at 80 kV acceleration voltage.

4.4 Statistical analysis (I–III)

Statistical analysis was accomplished by using JMP pro 16.2.0 (570548) in studies II–III. In the silica-modified alumina study (II), differences in the cell viability with materials were compared to the control group at each time point. Statistical significance was analysed by using the nonparametric multiple comparisons. Statistically significant differences between silica-modified alumina and alumina on same concentrations and time point were analysed by using Wilcoxon test with Bonferroni correction.

In the FCC study (III), cell viability in presence of FCC at each time point was compared to the respective control group. Statistical significance was analyzed by using the nonparametric multiple comparisons by Dunn methods for joint ranking. The same methods were used to compare calcium concentrations after incubating the samples with of different amounts of FCC particles. P-values < 0.05 were considered statistically significant.

5 Results

5.1 Physicochemical characterization of biomaterials (I–III)

Various physicochemical properties of materials, *i.e.* materials' vibrational features, crystal structure, morphology, dissolution behaviour, as well as release of ions and pH change were characterized. Vibrational features of the molecular structure of materials were characterized with ATR-FTIR. Peak assignments of the materials and ATR-FTIR spectra are shown in Figure 2.

Bioresorbable materials (HAP, CAP and FCC) showed strong absorbance at phosphate and carbonate wavenumbers. HAP showed strong absorbances at 563 cm^{-1} , 599 cm^{-1} , 635 cm^{-1} , 960 cm^{-1} , 1017 cm^{-1} and 1089 cm^{-1} , which are from phosphate molecule. CAP showed strong absorbance at 563 cm^{-1} , 602 cm^{-1} , 960 cm^{-1} and 1016 cm^{-1} , which are from phosphate molecule and also strong absorbance at 872 cm^{-1} , 1413 cm^{-1} and 1473 cm^{-1} , which are from carbonate molecule. FCC showed strong absorbance at 712 cm^{-1} , 874 cm^{-1} and $1\,427\text{ cm}^{-1}$, which are from carbonate molecule and one strong absorbance at $1\,023\text{ cm}^{-1}$, which is from phosphate molecule from the hydroxyapatite part of FCC.

The spectra of bioactive materials, *i.e.* BGs, indicated strong absorbances at $1006\text{--}1012\text{ cm}^{-1}$, $906\text{--}907\text{ cm}^{-1}$, and $731\text{--}746\text{ cm}^{-1}$, while BG 45S5 had also a strong absorbance peak at 847 cm^{-1} . The inert material alumina showed a broad absorbance peak at $500\text{--}750\text{ cm}^{-1}$. The silica modified alumina had wavenumber at 699 cm^{-1} (84% transmittance) and 1095 cm^{-1} (97% transmittance). However, no signs of silica on the alumina were found at wavenumber $650\text{--}2450\text{ cm}^{-1}$. Typically, signs of silica were found at wavenumbers 800 and $1\,100\text{ cm}^{-1}$.

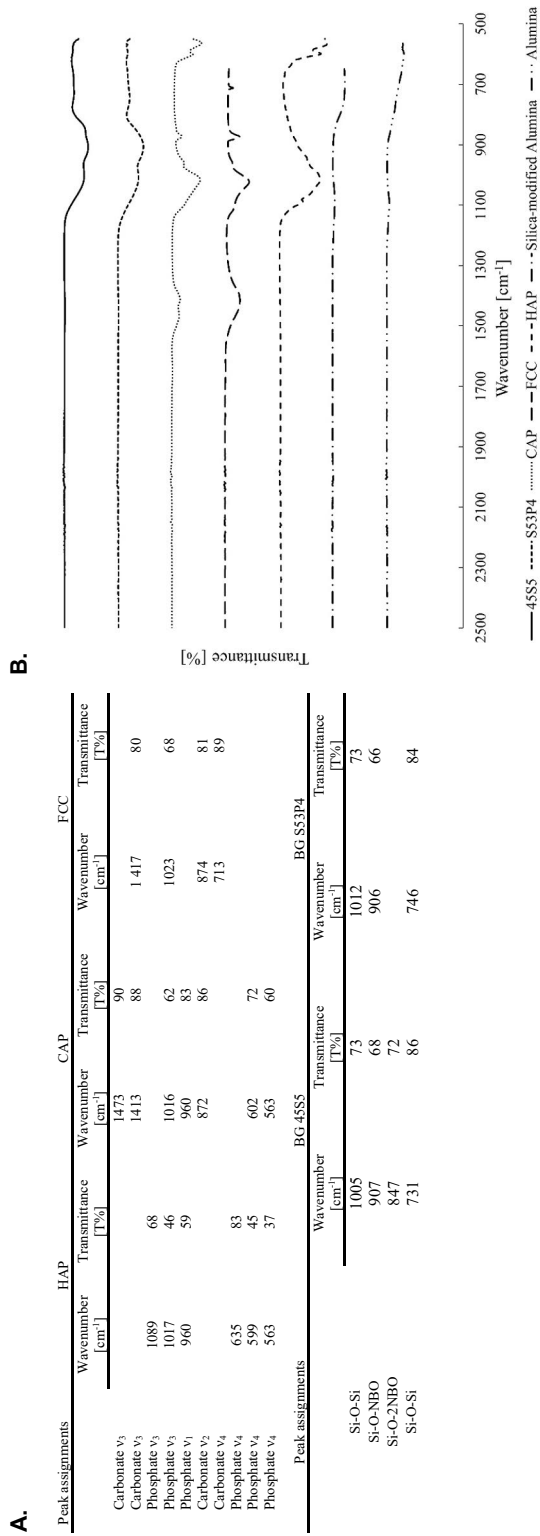


Figure 2. (A) ATR-FTIR peak assay. Identification of peak assignments is based on previous data by Hayashi et al., 2020; Joe et al., 1997; Madupalli et al., 2017; Rehman & Bonfield, 1997; Serra et al., 2003; Zheng et al., 2015. (B) ATR-FTIR spectra of the studied materials. Modified from original publication 1.

Crystal structures of the materials were characterized with X-ray Power Diffraction (XRD). The diffractograms of the materials are shown in Figure 3. The XRD patterns of bioresorbable materials, HAP and CAP, were equivalent to the standard data for $\text{Ca}_5(\text{PO}_4)_3(\text{OH})$ (ICDD card 00-009-0432) with some peaks matching the pattern of calcium phosphate whitlockite $\text{Ca}_3(\text{PO}_4)_2$ (ICDD card 00-055-0898). Comparison with reference data, it is clear that bioresorbable FCC has also hydroxyapatite (ICDD card 00-009-0432) and crystalline calcite (ICDD card 00-005-0586). Furthermore, XRD data also revealed a broad peak in the range of 9–18 degree 2Theta, which suggests that part of the FCC particles is of amorphous nature. The XRD patterns of bioactive materials, BG 45S5 and BG S53P4, showed broad peaks typical for amorphous materials.

The XRD pattern of alumina showed the main crystal phase to be corundum Al_2O_3 (ICDD card 00-010-0173), with some additional peaks, which can be indexed to either beta- Al_2O_3 (ICDD card 00-051-0769), or sodium alumina ($\text{NaAl}_{5.9}\text{O}_{9.4}$) (ICDD card 00-031-1262) or diaoyudaoite ($\text{NaAl}_{11}\text{O}_{17}$) (ICDD card 00-045-1451). XRD pattern of the silica-modified alumina has also the major crystalline phase equivalent to the standard data for the alpha- Al_2O_3 (corundum) phase (ICDD card 00-010-0173) with a minor contribution from the beta- Al_2O_3 phase (ICDD card 00-051-0769). In addition, both alumina and silica-modified alumina, also displayed a broad hump in the 10–20 2theta region, which indicates an amorphous phase. The XRD data also verified that silica-modified alumina had no crystalline SiO_2 .

Morphology of the material particles was analysed from SEM images at 50× and 30× magnifications, with the width and length of the image being 2.4×1.8 mm and 4.0×3.0 mm, respectively. SEM images showed that the particle morphology of BG 45S5, BG S53P4 and alumina was visually similar and that the particle surface was smooth. In contrast, the surface of bioresorbable materials HAP, CAP and FCC was porous (Figures 4 and 5).

Concentrations of elements at particles' surfaces were measured with x-ray analysis (EDXA) and then the oxide content of five materials (BG 45S5, BG S53P4, HAP, CAP and Alumina) was calculated. The predominant oxide for BGs (S53P4 and 45S5) was silicate (SiO_2), whereas the predominant oxides for the HAP and CAP were calcium oxide (CaO) and phosphorus oxide (P_2O_5). Alumina particles demonstrated aluminium oxide (Al_2O_3) with minor quantities of sodium oxide (Na_2O). The particle composition was close to oxide compositions stated by the manufacturer. However, some differences were perceived, *e.g.* impurities of alumina in BGs. The particle size was measured from the SEM micrographs and was shown to be the highest in BGs, around 800 μm , while the particle size of the three different alumina samples varied between 570 and 760 μm . CAP particle size was around 450 μm , while the HAP particles were the smallest, around 250 μm . All particle sizes and oxide compositions are presented in Table 12.

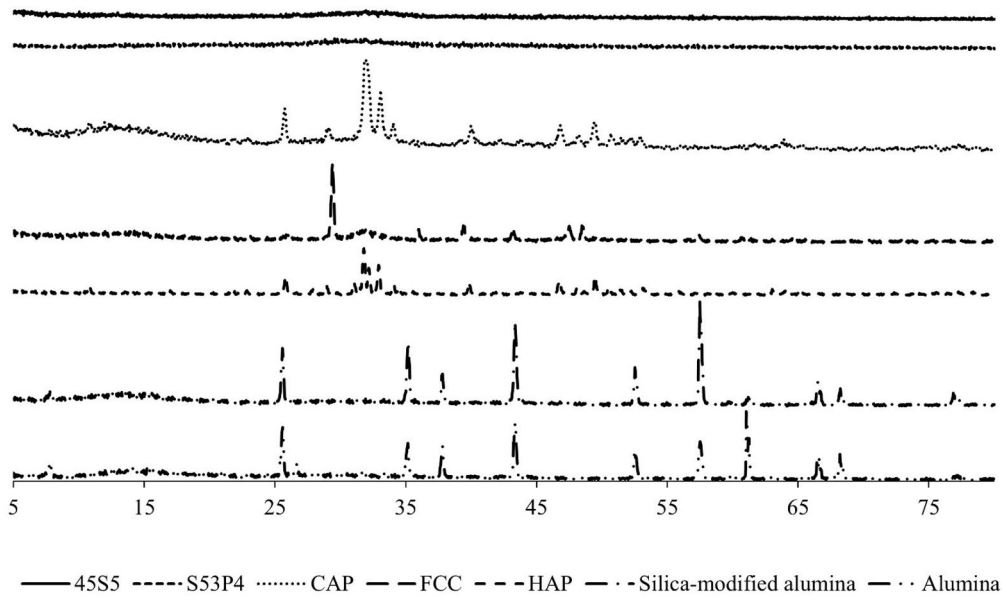


Figure 3. Structural characterization of studied materials with XRD. Modified from original publication I.

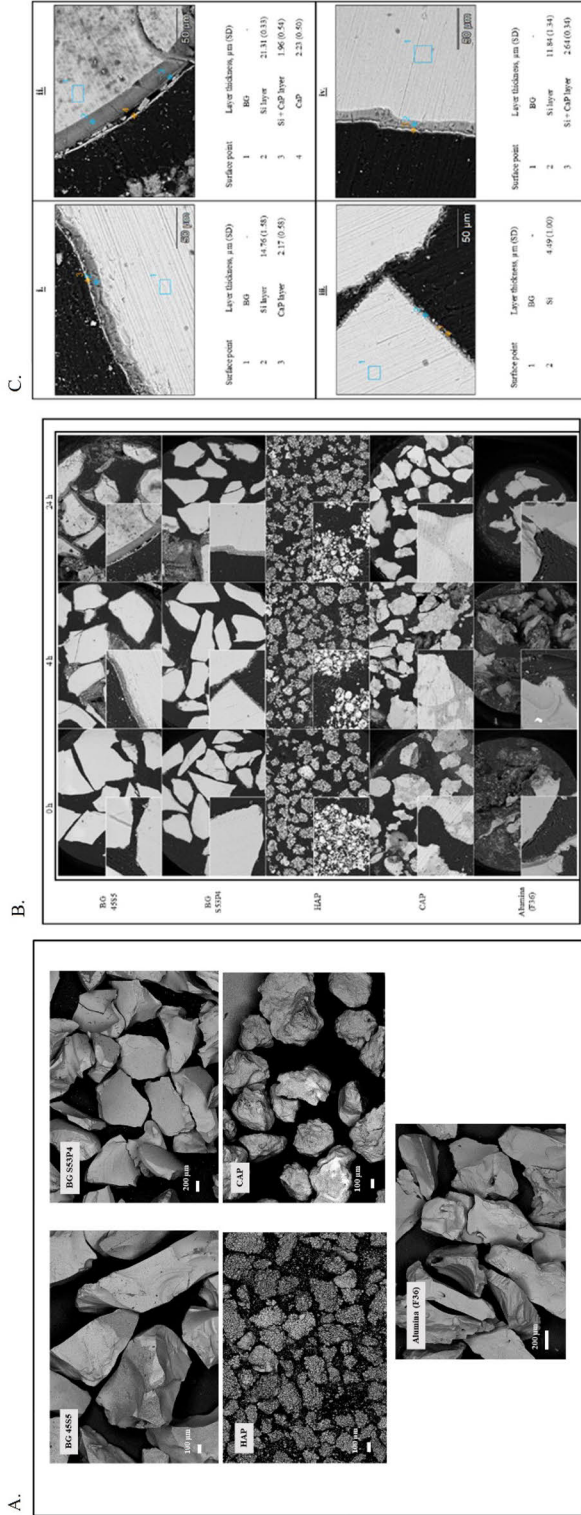


Figure 4. (A.) SEM images of the studied materials as received/before dissolution. (B.) SEM images of the cross-sectional surfaces of the studied materials after dissolution in continuous flow of in the Tris-buffer solution for up to 24 hours at 50 \times and 500 \times (left bottom corner) magnification, the width and length of the image being 2.4 \times 1.8 mm and 240 \times 180 mm, respectively. (C.) SEM micrographs showing the reaction layer thicknesses for BG-45S5 after 4 h (i) and 24 h (ii) and for BG-SS5P4 after 4 h (iii) and 24 h (iv). The EDX analyses give the elemental compositions of bulk glasses (points 1, 2) and surface layers (points 3 and 4). Si: silica rich layer; CaP: calcium-phosphate rich layer. Modified from original publication I.

Changes in the surface structure of clinically commonly used materials, BG 45S5, BG S53P4, HAP, CAP and alumina were characterized with SEM after 24 hours of continuous dynamic dissolution. SEM examination of particles showed formation of reaction layers at the surfaces of BG 45S5 and BG S53P4 during the 24 hours of the continuously dynamic dissolution (Figure 4B and C). According to the SEM-EDX analysis after dissolution, the thickness of the silica-rich reaction layer grew from around 15 μm at 4 hours to 21 μm at 24 hours for BG 45S5. The corresponding layer thickness of BG S53P4 was 4 μm at 4 hours and 12 μm at 24 hours. The outermost part of the reaction layer showed the presence of calcium phosphate for both BGs. However, no reaction layer was seen by the SEM examination at HAP, CAP or alumina. In addition, bioresorbable material FCC the reaction layer was studied, but because of the particle small size, the reaction layer was not detectable.

Silica modified alumina's surface changes were studied only in static dissolution because of the small quantity of silica in silica-modified particles. The static analysis was done in Tris buffer and SBF. SEM images at different magnification of the silica-modified alumina particles are shown as received and after 24 hours of static dissolution in Tris buffer and SBF (Figure 5 I). For magnifications of 1000 X, 5000 X and 25000 X, the surface areas indicated are $120 \times 90 \mu\text{m}$, $24 \times 18 \mu\text{m}$, $4 \times 3.6 \mu\text{m}$, respectively. No changes of the particle morphology were visually seen in SEM images before or after static dissolution tests regardless of dissolution time (0-24h). SEM-EDXA of randomly selected areas of silica-modified alumina particle (before dissolution) gave silica concentrations between 0–42%, indicating that the silica was not evenly covering the alumina surface (Figure 5 III). The silica particles were shown to be about 100 nm spherical nanoparticles above the alumina layer (Figure 5).

FCC particles' surface changes was studied in a static dissolution system in cell culture setting to represent biological conditions. SEM examination of FCC particles was made as received and after 14 days of cell culture medium dissolution. SEM images were obtained with 2.5 kX, 10 kX, 25 kX magnifications, the dimensions of the images being $46 \times 36 \mu\text{m}$, $12 \times 9 \mu\text{m}$ and $4.8 \times 3.6 \mu\text{m}$, respectively. FCC particles without any dissolution had a fine porous surface structure and they varied in size (Figure 5 II, left-hand panels). After 14 days of dissolution in the cell culture medium, the particles' surface porosity decreased (Figure 5 II, right-hand panels), probably due to adhesion of proteins present in cell culture medium.

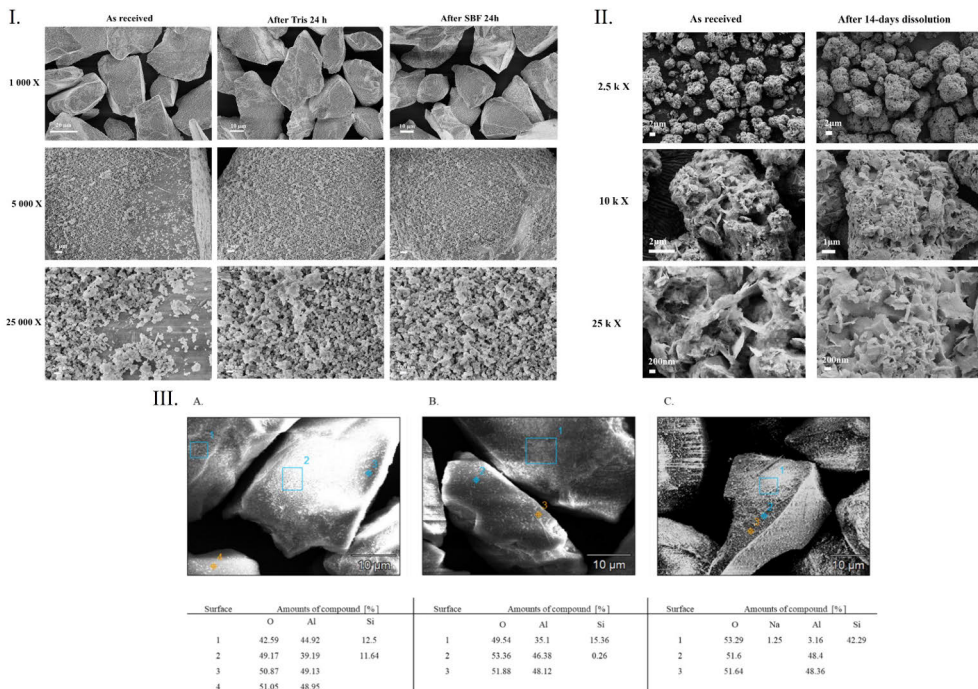
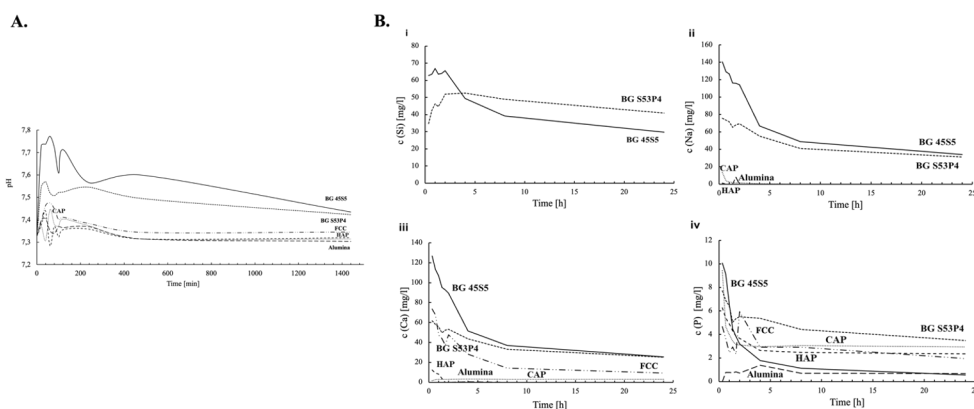


Figure 5. I. SEM images of the silica-modified alumina before (“As received”) static dissolution test in the Tris-buffer solution and after the static dissolution test in Tris-buffer in SBF (“After Tris / SBF 24h”). II. The FCC surfaces as examined by SEM The FCC surface as received (left-hand panels) in original magnifications were and scale bars 2.5 k X/2µm, 10 k X/2 µm, 25 k X/200nm. The FCC surfaces after being immersed in cell culture medium up to 14 days (right-hand panels) in original magnifications were and scale bars 2.5 k X/2µm, 10 k X/1 µm, 25 k X/200nm. III. Areas of SEM-EDX analysis of the silica-modified alumina surface for detecting presence of silica on the surface. Modified from original publication II–III.

Biomaterials’ pH change and ions dissolution was studied in a continuous dynamic system in Tris buffer (Figure 6). pH and released ions were measured as a function of immersion time of the dissolution test. An increase of the pH of the immersion solution was shown especially for BG 45S5 and BG S53P4 within 50 to 100 minutes, followed by a minor drop, after which the pH increased again at around the time point of 100 minutes (Figure 6A). Finally, the pH of the immersion solution of the BGs gradually decreased. The four other materials, HAP, CAP, FCC and alumina caused only minor increases (pH unit of 0.1) in pH during the first 50 to 100 minutes of immersion. Then, the pH of the solution was at the same level as in the fresh solution fed into the reaction.

Table 12. Oxide compositions (w%) and mean particle sizes of the biomaterials based on SEM-EDX analyses. Original publication I.

Materials	Particle size (diameter) μm (SD)	Compositions %					
		Na ₂ O	Al ₂ O ₃	SiO ₂	P ₂ O ₅	CaO	MgO
BG S53P4	842 (52)	25.78	0.28	49.60	3.86	20.49	
BG 45S5	822 (110)	29.31	0.17	40.12	5.08	25.32	
CAP	445 (150)	5.26	1.03		39.14	54.57	
HAP	251 (24)		0.37	0.31	40.18	58.78	0.36
Alumina	574 (28)	1.74	98.26				

**Figure 6.** pH changes of the studied materials in Tris-buffer solution as the function of dissolution time (A). Dissolution of ions from the studied materials into Tris-buffer solution as the function of time (B). i. silicon, ii. sodium, iii. calcium, iv. phosphorus. Modified from original publication I.

Ion dissolution analyses showed clear differences between the materials (Figure 6B). The bioactive materials BGs 45S5 and S53P4 showed a rapid initial release of sodium and calcium ions, followed by the release of silicon species. Then, the ion concentrations gradually decreased but stayed at relatively high levels throughout the 24 hours of experimental time.

Minor initial release of sodium ions was registered for HAP, CAP and alumina, most likely due to Na₂O impurity. Calcium ion release from bioresorbable materials CAP, HAP and inert alumina was very low but constant over the experimental time, while only a minor initial dissolution was measured for HAP. However, bioresorbable FCC showed a high release of calcium.

The release of phosphorus from the materials was on a much lower level. After the higher initial releases during the first hours, the concentration of phosphorus decreased to clearly lower levels for BG S53P4, HAP, FCC and CAP. In contrast, the phosphorus concentration released from BG 45S5 after the first hours was below

the level of quantification (LOQ), as well as for the phosphorus-free alumina during complete experimental time.

In addition to the continuously dynamic system, FCC material's pH change and ion release were studied in a static system with water or cell culture medium. In addition, the static dissolution system was performed by either changing the fluid (water or cell culture medium) during the experiment (similarly as for cell viability experiments) or without any liquid changes.

In the static dissolution system with FCC in cell culture medium, pH remained approximately the same (7.3–7.4) during the follow-up time, irrespective of whether the medium was changed in-between or not (Figure 7C–D). However, small differences were shown in the system, where the cell culture medium was changed every 3–4 days during the 14-day follow-up. In water, pH change differed from that of the cell culture medium, most likely due to media's buffering capacity. When the water was unchanged during the follow-up, the pH value increased in the beginning of immersion and, was then followed by stabilization at around day one with highest concentrations (200 µg/ml) of FCC (Figure 7A). In the system, where water was changed every 3–4 days during the follow-up, the pH decreased gradually over time (Figure 7B). All of the four systems showed minor peaks at the same time points, which were the times, when the plate was taken out from the incubator and the cell culture medium or water was changed in certain wells.

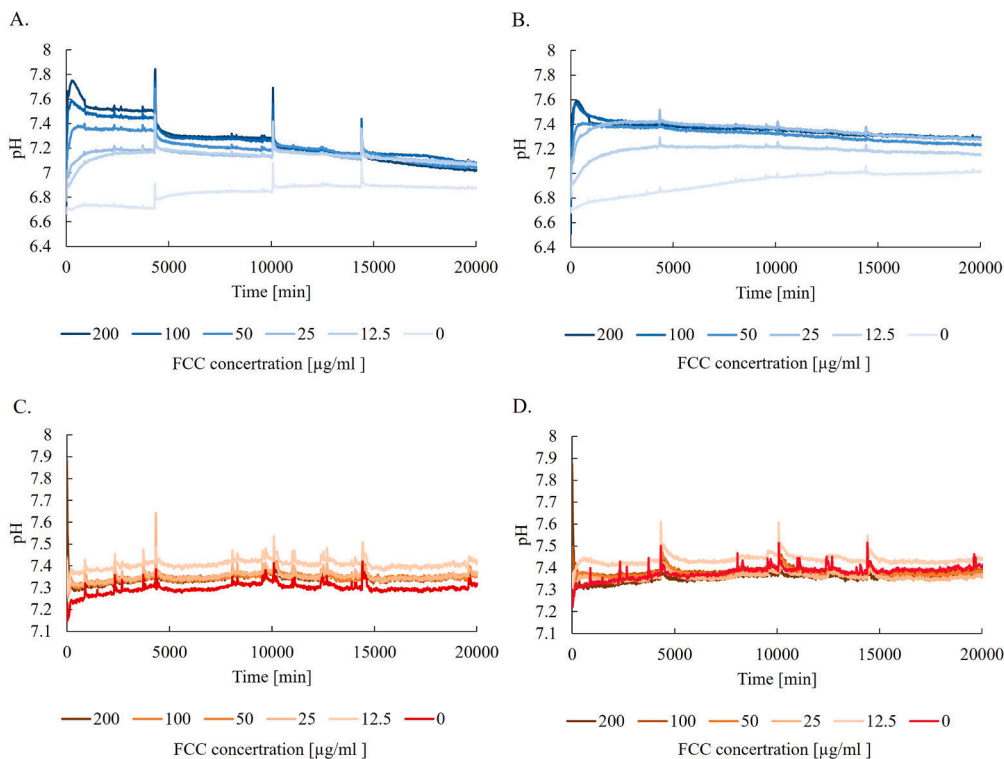


Figure 7. pH changes of the Tris-buffer solution as functions of dissolution time in the studied materials. (b) Dissolution of ions from the studied materials into Tris-buffer solution as function of time. i. silicon, ii. sodium, iii. calcium, iv. phosphorus. Original publication III.

After 14 days of dissolution, calcium concentration of the cell culture medium was significantly decreased in the presence of FCC at 200 µg/ml if the cell culture medium had not been changed during the follow-up period ($P < 0.05$, Figure 8A). In the system, where the cell culture medium was changed every 3–4 days, no significant differences were observed in calcium concentration. In the system, where water was not changed, the calcium levels were below the detection limits of the analysis method (< 1 mg/L) and were reliably measurable only when FCC concentration was higher than 50 µg/ml. However, when the liquid was changed, dissolved FCC was probably removed during changing of the water and no calcium was detectable (Figure. 8B).

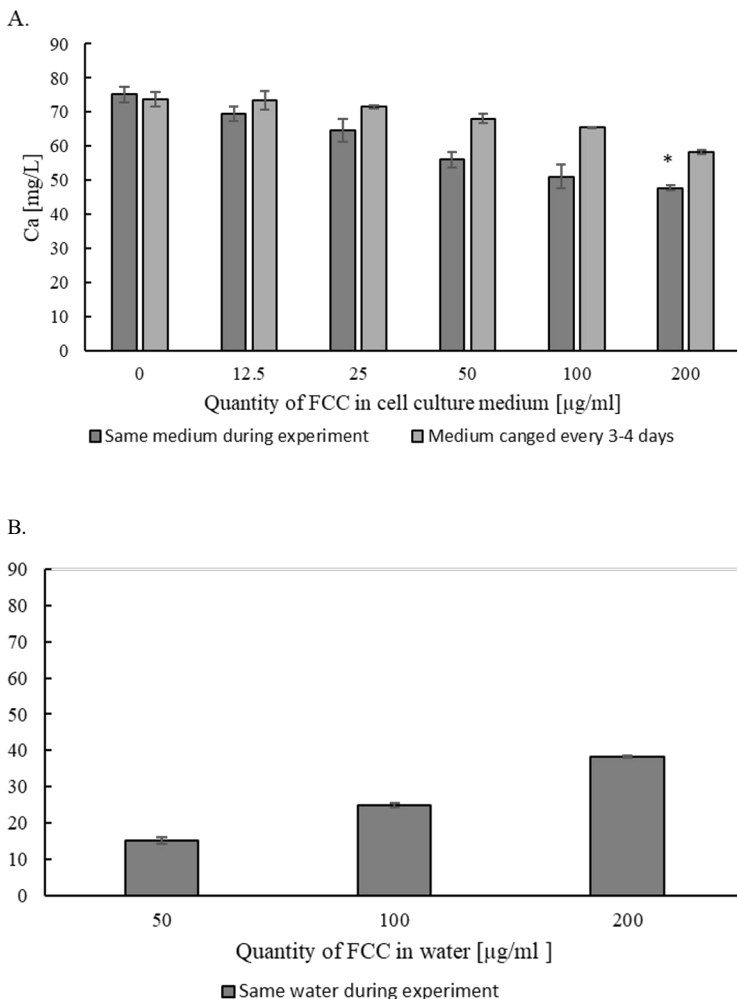


Figure 8. Concentration of calcium in static dissolution system. **(A)** Concentration of calcium in cell culture medium and **(B)** in water in the static system after 14 days of FCC dissolution. Data are presented as an average \pm SD ($n=2$), * $p < 0.05$ vs. control group 0 $\mu\text{g/ml}$. Original publication III.

Silica-modified alumina’s pH change and ion release was measured in a continuous dynamic system in Tris buffer and in addition in a static system in Tris buffer or in SBF. In SBF static dissolution test, the pH variation was minor, about 0.06 pH unit, and a similar observation was made in both the continuous and static systems with Tris buffer, where the variation in pH was also minor, only 0.04 and 0.07 pH units, respectively.

In the continuous dissolution system, some Na, Ca, and P ions were released from the silica-modified alumina particles during the first two hours. No other ions were

detected. In the static dissolution system into Tris-buffer, the ions were below the detection limit. In contrast, Si was released from the silica-modified alumina into α -MEM at increasing particle concentration and with prolonged immersion time (Figure 9).

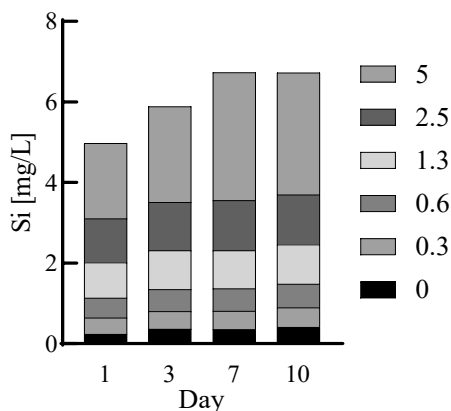


Figure 9. Si release to α -MEM with different silica-modified alumina particle concentrations at different immersion times. Original publication II.

5.1 Biological characterization of biomaterials (II–III)

The bioresorbable FCC and silica-modified alumina, which are not yet clinically used, were, in addition to physicochemical properties, also biologically characterized. Biological characterization was performed with a well-established pre-osteoblastic mouse cell line MC3T3-E1 and cell viability was evaluated in the presence of silica-modified alumina, alumina and FCC particles.

No differences were observed in the viability of pre-osteoblastic cells between silica-modified alumina and alumina (Figure 10A, B). However, cell viability was significantly decreased ($P < 0.05$) in the presence of alumina at 5 mg/ml on day 10 ($P=0.0066$), when compared to the control group on same day. Cells were also visually inspected under the light microscope during the 10-day culture period but no major effects on cell morphology were observed (data not shown).

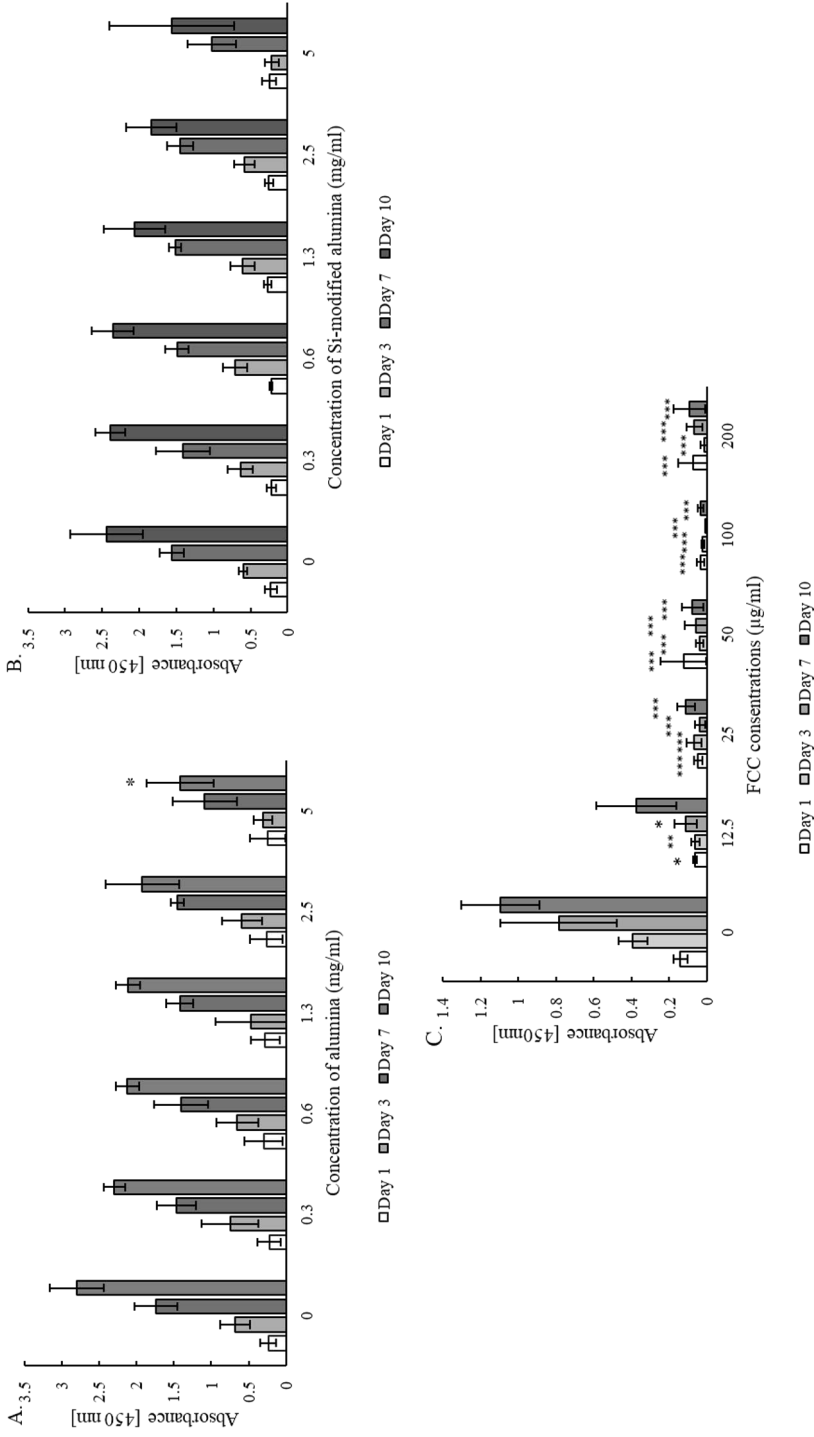


Figure 10. MC3T3-E1 cell viability assayed with WST-method (450 nm) with different concentrations of silica-modified alumina (A), alumina (B) and FCC (C) particles. Data are presented as an average \pm SD (n=3), *p < 0.05, **p < 0.01, ***p < 0.001 vs. control group 0 μ g/ml at respective time point. Please note that the methods used in c were different than the ones used in a and b. Modified from original publication II–III.

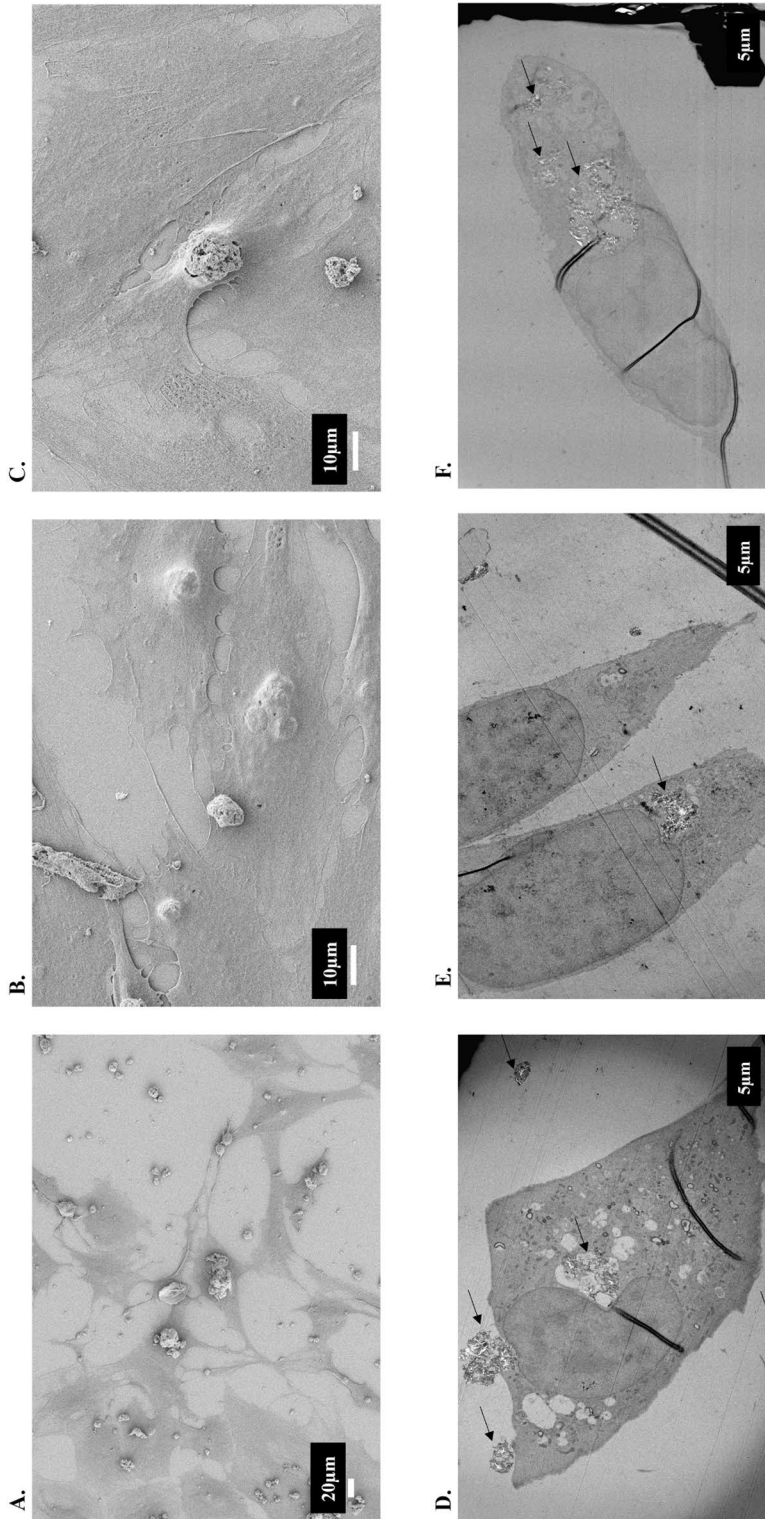


Figure 11. (A.-C.) SEM and (D.-F.) TEM images from MC3T3-E1 cells cultured with FCC particles (12.5 $\mu\text{g}/\text{ml}$ or 25 $\mu\text{g}/\text{ml}$) on day 10 of cell culture. In D-F, intracellular FCC particles are annotated with black arrows. Original publication III.

However, FCC particles affected pre-osteoblastic cell viability, which was significantly decreased ($P < 0.05$) in the presence of FCC particles (12.5, 25, 50, 100, 200 $\mu\text{g/ml}$) at all concentrations and time-points, except for day 10 time point with FCC at 12.5 $\mu\text{g/ml}$ (Figure 10C). Pre-osteoblastic cells proliferated normally in control wells (*i.e.* without FCC particles) and visual inspection with a light microscope over the 14-day culture period confirmed normal cell proliferation and morphology in wells without FCC (data not shown). In addition, light microscopy implicated that FCC particles were located within MC3T3-E1 cells, which led us to closer investigations using SEM and TEM imaging.

SEM and TEM images were taken of MC3T3-E1 cells cultured in the presence of FCC particles (12.5 $\mu\text{g/ml}$ and 25 $\mu\text{g/ml}$) for 10 days. Both imaging methods showed that MC3T3-E1 cells had internalized FCC particles, since FCC particles were observed both intracellularly (Figure 11B, 11D–F), as well as outside the cell and on the plasma membrane (Figure 11A, 11C–D).

6 Discussion

Different materials, *i.e.* natural bone and synthetic biomaterials have been used for bone repair. Despite of long-term development and studies on different biomaterials, more research is still needed. In addition, new materials and different material compositions need detailed investigations before they can be clinically applied. Knowledge on the biomaterials' physicochemical properties is a prerequisite for biological studies, because physicochemical properties, such as surface crystal structure, topography and roughness are known to affect cell attachment, proliferation and differentiation, as well as re-precipitation of minerals from materials' microenvironments (Anada et al., 2008; Choi et al., 2020). In this thesis, commonly used bioceramics and some new bioceramics in the field of bone repair were compared physicochemically. Clear differences were shown in their properties, which have been described to be biologically relevant. For the first time, we studied FCC and silica-modified alumina bioceramics for bone repair. The silica-modified alumina did not show significant effects to cells, in contrast to FCC, which inhibited cell viability and proliferation.

The different biomaterials' molecular bonding has been previously evaluated by ATR-FTIR. CAP has two different chemical structures, which depend on carbonate substituting group. In type A, carbonate is substituting for OH⁻ and in type B for PO₄³⁻. We observed carbonate's double bounds of the third vibrational modes at 1413 cm⁻¹ and 1473 cm⁻¹, which indicate CAP to be of both A and B type (Hayashi et al., 2020; Madupalli et al., 2017). The carbon type affects synthetic biomaterials' crystallinity and solubility (Madupalli et al., 2017). Theoretically, carbonate ions have four vibrational modes, but in our study, we observed two of these vibrational modes, probably due to sensitivity of analysis (Rehman & Bonfield, 1997). The phosphorous ions also have four vibrational modes, while we observed only the first, third and fourth vibrational modes (Rehman & Bonfield, 1997). In turn, the second modes are unusually weak (Rehman & Bonfield, 1997). HAP and CAP include a hydroxyl ion, which has a vibration mode over 3550 cm⁻¹ (Madupalli et al., 2017; Rehman & Bonfield, 1997). Unfortunately, we did not observe that because of our wavenumbers scale. The bioinert alumina was observed to have octahedral vibration

bands of Al-O at 500–750 cm^{-1} , similar to silica-modified alumina particles (Joe et al., 1997).

BG 45S5 and S53P4 showed mainly similar chemical compositions of bonding, except for variations in BG's amorphous structure. This was caused by network modifiers which consist of silicate and phosphorus (Serra et al., 2003; Zheng et al., 2015). The silicate network modifiers in low to high glass network vary in content of silicate, which can range from non-bridging to tetrahedral (Brauer & Möncke, 2017; Serra et al., 2003). In our ATR-FTIR studies, two silicate non-bridging oxygen groups at 849 cm^{-1} were seen only in BG 45S5 which had lower silica content and not BG S53P4 which had higher silica content. The network formation is known to impact BG's ion release, solubility, degradation, and bioactivity (Brauer & Möncke, 2017; Serra et al., 2003). This was also observed in our dissolution test in Tris buffer, when BG 45S5 showed surface reactions more quickly than BG S53P4 with a higher network formation.

In our dissolution study in Tris buffer, the BGs increased pH value more than other studied materials. In addition, BGs differed from each other, since BG 45S5 showed higher pH during the immersion than BG S53P4. These higher pH values correlate with higher antibacterial properties (Vallittu, 2017; Vallittu et al., 2015). pH increase by both BGs can be caused by high release of sodium and calcium ions from BGs. The BG's pH curve showed two increases at the time points of 50 and 100 min followed by a minor drop. Such minor variations in pH curve have also been previously reported (Fagerlund et al., 2013).

Ion release from BG has previously been shown to stimulate expression of osteogenic growth factors and also other genes relevant for cell attachment, proliferation and differentiation (Björkenheim et al., 2019; Fagerlund & Hupa, 2017; Hoppe et al., 2011; Jones et al., 2016). However, it has to be taken into account that different concentrations of released ions and balance between these ions should be optimal for the osteogenic effect. Both of BGs showed similar dissolution curves for calcium and sodium ions but had differences in silicon and phosphorus dissolution release. The higher silicon content was seen at the beginning of dissolution with BG 45S5 and at the last four hours with BG S53P4. The phosphorus dissolutions from BGs were different. The phosphorous ion release from BG 45S5 decreased inversely but BG S53P4 showed more variation and higher content during the follow-up period.

Previously it has been reported that optimal ion concentrations for osteostimulation would be 20 ppm for silicon and 60–90 ppm for calcium (Hench, 2009; Hupa, 2018). In general, our BG dissolution test and pH change are in line with previous studies (Fagerlund et al., 2013; Hupa, 2018; Jones et al., 2016; Vallittu, 2017). However, there are some differences. For example, we showed higher concentrations of calcium and silicon dissolution from BGs than previous

studies but these higher levels were observed only within the first hours. This might be explained by the different dissolution time (24 h) compared to previous studies (1 000 s). It is also possible that the particle size has been different in these studies (Fagerlund et al., 2013). BGs ion dissolution has an important effect in the surrounding tissues, as ion concentrations and pH change are known to contribute *e.g.* to materials' antibacterial properties (Zhang et al., 2010). High changes of these parameters can induce toxic effects, while optimal leaching of calcium and phosphorous ions can induce ossification (Fagerlund & Hupa, 2017; Monfoulet et al., 2014).

All similarly characterized biomaterials (BG 45S5, BG S53P4, HAP, CAP, FCC and Alumina) showed different ion dissolution profiles. In general, other biomaterials than BGs showed low ion dissolution. Previous studies have shown low calcium ion dissolution with HAP compared to CAP (Ishikawa, 2019). Via low ion dissolution, CAP appears to be more osteoconductive than HAP, which may be caused by the ability of osteoclasts to resorb more CAP. The bioinert alumina was shown to increase the pH and dissolve minor quantities of sodium and phosphorus in the beginning of dissolution in Tris buffer. These ions may be traces of the alumina particles. However, no aluminium ions were detected.

Material properties, such as material surface properties have been improved by different surface modifications. For example, biomaterials covered by another biomaterial can improve interactions via protein adsorption and cell attachment to biomaterials' surface. These kinds of biomaterials, *i.e.* FCC and silica-modified alumina, were studied in this thesis.

The FCC particles were physicochemically and biologically characterized as a possible bone restoration material. The physicochemical characterization showed that FCC particle consists of a CC core and HAP surface. The HAP surface contains first a 100 nm porous meshwork and then 1 μm thick lamellar structure of HAP. The lamellar structure is responsible for the mechanical stability and interlocking of FCC as previously reported (Roth, 2019). Our SEM analysis showed this porous structure. In our ATR-FTIR analysis, adsorption bands of carbonate at 713 cm^{-1} (ν_4), 874 cm^{-1} (ν_2) and 1417 cm^{-1} (ν_4) were seen in addition to the bands of phosphates at 1023 cm^{-1} (ν_3), which originate from the hydroxyapatite part of FCC. These results and XRD confirm that CC is of stable calcite form.

FCC did not change pH value in buffered systems (cell culture medium or Tris-buffer), where the pH value remained approximately the same during the follow-up time, but uniquely the pH increased at the beginning of immersion in the water dissolution. In Tris buffer and water immersion, calcium ions were released, thus the CC was anhydrous form of stable calcite. However, the K_{sp} value of HAP is much lower than that CC, which explains high calcium levels from the CC part of FCC in the immersion systems. In addition, the carbon dioxide in the atmosphere of

immersion system affects calcium dissolution K_{sp} values. Interestingly, FCC particles were observed to adsorb calcium ions from cell culture medium, which is in line with data from previous studies on nanometer-size CC, as well as with the data showing that calcium phosphate with a high surface microporosity can strongly adsorb proteins (Horie et al., 2014; Samavedi et al., 2013).

Material's solubility, surface change and ion microenvironment all influence cell behavior (Samavedi et al., 2013). Thus, the ability of FCC to bind calcium led us to study, whether the change of media would cause variation in the biological test, as cell viability was assessed *in vitro*. However, we did not observe that the change of medium would affect calcium concentrations.

In the biological characterization, we found out FCC inhibited the pre-osteoblastic cell viability at all FCC concentrations, which were included. Previous studies with nanoscale CC particles and human MSCs are in line with our FCC study (Li et al., 2018). Furthermore, HAP particles of various sizes have been shown to have negative effects on osteoblast viability and growth factor secretion (Sun et al., 1998). However, there is also studies with opposite results. Biomaterial's ability to adsorb calcium have in some cases been reported to have beneficial effects on cell differentiation and proliferation and affect certain kinase pathways (Samavedi et al., 2013). In addition, nanoscale CC has been reported to stimulate osteogenic cell differentiation (Li et al., 2018). Although there is contradictory data, coralline CC and HAP have been used in implantable materials with good results *in vitro* and *in vivo* (Fu et al., 2013; Jamali et al., 2002; Ong et al., 2012; Ripamonti et al., 2009; Walsh et al., 2003).

Interestingly, in our study the pre-osteoblastic MC3T3-E1 cells were shown to internalize FCC particles, probably via phagocytosis. This result is line with previous studies, where similar results have been obtained with HAP particles and MC3T3-E1 cells, human osteoblast-like cells and MG-63 cell line (Alliot-Licht et al., 1991; Lohmann et al., 2000; Moerke et al., 2016). The ability of osteoblasts, which normally are not considered as phagocytotic cells, to internalize such micrometer-scale biomaterial particles *in vivo* remains unknown. However, such a behavior of microscale surface-active biomaterial has to be considered in cell culture testing *in vitro*. The fusion of HAP and CC into FCC should lead to one cohesive particle without decomposition into smaller particles. However, the possible effects of FCC surface microporosity and micromechanical properties on cell viability and differentiation still remain unclear.

FCC's ability to adsorb calcium from the cell culture medium most likely limits the cell viability *in vitro* because calcium is an essential element for cell functionality and viability. In addition, the ability of pre-osteoblastic cells to phagocytose FCC particles and their degradation products can also limit cell viability. However, such phagocytotic activity and the consequences of FCC's ability to adsorb calcium in *in*

vivo environments remain unknown. Nonetheless, as long as these effects are unclear, and as FCC demonstrated negative effects on cell viability more careful *in vitro* studies are needed to evaluate the possible potential of FCC in bone applications.

Another biomaterial, which was studied for the first time in the context of bone repair, was the silica-coated material that has been originally developed for dentistry to improve adhesion of tooth substance via tribochemical silica coating. The coating method is based on silica-modified alumina particles, which are air-blown in the tooth substance, where these particles create a clean surface and optimal wettability by increasing hydroxyl groups via silica layer on substance surfaces (Martins et al., 2019; Thammajaruk et al., 2018). In other words, silica-modified alumina particles can form silica layer to tooth substance – a phenomenon, which has previously been extensively studied (Abi-Rached et al., 2014; Galvão Ribeiro et al., 2018; Hjerppe et al., 2016; Khan et al., 2019; Martins et al., 2019; Özcan & Vallittu, 2003). However, silica-modified alumina particles are less well characterized and it is possible that the dissolution of silica can have cellular effects in other contexts, such as on bone cells (as described in chapter 2.1.3.2.) The silica-derived biomaterials, e.g. zeolite and silicon-substituted calcium phosphate derived silicate, have been shown to have positive effects on bone health and sodium metasilicate has been reported to affect pre-osteoblastic cells, although the effect of silica ions on osteogenic cells is not yet completely understood (E. J. Kim et al., 2013; W. Wang & Yeung, 2017; Zhou et al., 2017). In addition, the studies of silicon-substituted calcium phosphates have lack of evidence of silicon release and material resorption rates. Thus, these results have been critically discussed. In this thesis, three different dissolution methods were used to study silica ion dissolution from the silica-modified alumina particles.

The ultrastructure of silica-modified alumina has been previously studied and it was shown that the silica layer is 50nm thick and silica is present as small agglomerates on the surface of alumina (E. J. Kim et al., 2013). Our SEM-EDX analysis is in line with this study. However, our study did not confirm, whether the silica was amorphous and potentially porous in order to dissolve. After 24 h of silica-modified particle immersion in static SBF and Tris buffer or in continuous Tris buffer flow no significant signs of dissolution or pH changes were detected. These results were also confirmed by SEM observations. Interestingly, silica ions were detected, when silica-modified alumina particles were immersed in the cell culture medium (without FBS) and the ion concentration increased along the particle amounts and over prolonged immersion time. These results led us to study the effects of silica-modified particle on pre-osteoblast cell viability.

The concentration of silica released in α -MEM was quite close to the previously studied concentration of sodium metasilicate (0.5–2.5 mg/L), where silica was

reported to affect pre-osteoblast viability, differentiation, and mineralization (E. J. Kim et al., 2013). Interestingly, in the viability test, the silica-modified particles had no effect on the viability of pre-osteoblastic cells. The differences between these results suggest that the release of silica in α -MEM can differ from dissolution in a cell culture setting (where α -MEM is supplemented with FBS). In addition, in previous studies the sodium silicate was aqueous, not solid in a biomaterial. In our study, same size alumina and silica-modified alumina particles did not show any significant differences in cell viability, except for a decreased viability on day 10 in the presence of 5 mg/ml of alumina. This was however not observed with silica-modified alumina, which may be explained by its silica content.

The silica nanoparticles have been previously shown to stimulate osteoblast differentiation and mineralisation but do not affect osteoclastogenesis or osteoclast viability (Beck et al., 2012). The particle, which was used in the study by Beck et al., was of the same size as our silica-modified alumina particle and the results are in line with our results. In addition, previous studies have shown that silicon doping of alumina tubes can stimulate cellular activity at tubes interface *in vivo* but also that even though 5 mol. % of silica enhanced osteogenesis, the osteogenic maturation was impaired in the presence of 0.5 mol. % of silica.

We studied the biomaterial particles' chemical properties with SEM-EDX. Also, the silica-modified alumina particle, which consist of two materials was studied with the same method. However, this characterization method was not optimal for elemental analysis because of two materials overlapped.

The studies addressing biomaterials dissolution properties are not mutually comparable. Each of these dissolution tests showed material properties for this specific environment, *i.e.* static dissolution showed silica ions to dissolve out of silica-modified alumina particle, which was not seen in continuous dissolution. The static dissolution demonstrated that low content of silica is capable of dissolve out of silica-modified alumina particle in a similar environment, where biological characterization was performed. The dissolution test with FCC material in an incubator showed minor peaks at the time-points when plate was taken out of incubator. The pH peak was detected in all samples irrespective of if the dissolution media was changed or not. These results indicate that change in CO₂ (g) atmosphere caused this effect and not the change of media. These different dissolution studies indicate that the microenvironment considerably influences the physicochemical and biological characterization of biomaterials and must be taken into account, when planning and executing the experiments. Different methods should be carefully considered, when the results from various *in vitro* studies are being interpreted. In addition, it should be noted that the *in vivo* situation with blood circulation resembles a continuous system and thus a cell culture setting with such a system might be closer

to *in vivo* environment. This aspect provides an interesting starting point for the biological characterization of biomaterials in the future.

FCC has been previously studied in drug delivery systems, where the ability of a biomaterial to adsorb drug molecules is an essential property (Roth, 2019). This could also explain our results, which showed that FCC adsorbed calcium from the cell culture medium. In our *in vitro* study, this property caused negative effects on pre-osteoblast cell viability, which however may not necessarily be as strong in an *in vivo* environment. For example, hydroxyapatite has shown a similar negative effect in previous studies, but it has still been used as a successful material for bone repair. However, all this highlights the need for further studies. In addition, these properties could possibly be studied for the local delivery of calcium or bone-active drugs to enhance bone repair in the future. However, all this warrants further studies both from the biological and biomechanical perspectives.

The silica-modified alumina had no effects on pre-osteoblast cell viability, even though silica has been reported to increase pre-osteoblast cell differentiation and mineralization (Beck et al., 2012; Pabbruwe et al., 2004). This indicates that silica-modified alumina could have positive effects to bone formation both *in vitro* and *in vivo*. In addition, the effects and possible mechanisms of biomaterials' dissolution products on cell viability, differentiation, mineralization etc. warrants further studies.

In summary, the physicochemical characterization of biomaterials showed differences between various biomaterials, which could impact their suitability in biological settings and influence the selection of an optimal biomaterial for bone repair. In addition, in this study, we studied two new bioceramics on the context of bone repair, but further studies are required before these two materials could possibly be clinically used.

7 Conclusions

Based on the physiochemical and biological characterization of different biomaterials in this *in vitro* study, following conclusion can be drawn:

1. All characterized biomaterials differed from each other in their physiochemical properties, such as ion release and pH change. These properties have impact on suitability of biomaterials in the biological settings and when choosing an optimal biomaterial for bone repair.
2. Minor quantities of silicate ions can be dissolved from silica-modified alumina *in vitro* in α -MEM. However, no dissolved silicate ions were detected in SBF or Tris buffer.
3. Alumina and silica-modified alumina counterpart showed no major effects or differences in pre-osteoblast cell viability.
4. FCC can adsorb calcium ions from α -MEM.
5. FCC decreases pre-osteoblastic cell viability, and in addition, FCC was shown to be internalized by these cells, which are not normally considered as phagocytosing cells.

Acknowledgements

This thesis was carried out at the Department of Biomaterials Science and Turku Clinical Biomaterial Centre TCBC, at the Institute of Dentistry, University of Turku Finland during the years 2019–2023. The study was supported by the Finnish Doctoral Programme in Oral Sciences (FINDOS) and foundations of the Academy of Finland Grant (ADMIO #323596) and Finnish Dental Association Apollonia student grant. This thesis was carried out concurrently with my DDS studies. This would have not been possible without excellent supervision, cooperation and support for scientific work from my supervisors, co-authors, and follow-up committee members.

I want to express my gratitude to the following people:

Professor Pekka Vallittu for excellent supervision and inspiring me into scientific work and sharing extensive knowledge of biomaterial science. I'm especially grateful for his swift responses to any scientific question I have had.

Adjunct professor Terhi Heino for excellent supervision, sharing extensive knowledge of cell cultures, and well-reasoned and critical views to the research questions.

I could not have asked for better supervisors than Pekka and Terhi. I want to thank both of them for trust and believing me as a doctoral researcher.

Follow-up committee members Professor Timo Närhi and Professor Leena Hupa for sharing scientific knowledge. I would also thank Professor Leena Hupa as a co-author for contribution and experience in bioactive glass and biomaterial characterization.

All co-authors, Professor Jouko Peltonen, Adjunct professor Jan-Henrik Smått, M.Sc Minna Siekkinen, M.Sc Syeda Qudsia, Adjunct professor Miho Nakamura, Wolfgang Hoepfl, and Tanja Budde for contribution and sharing scientific knowledge. Especially, I would like to thank the co-authors from Åbo Akademi for their quick responses to my scientific questions.

M.Sc Linus Silvander for SEM analyses and PhD Luis Bezerra for ICP-OES analyses. Electron Microscopy Laboratory, Institute of Biomedicine, University of

Turku, which receives financial support from Biocenter Finland, for EM cell sample processing and analysis.

Adjunct professor Vuokko Loimaanranta for experience in pH measurements and sharing scientific knowledge. Technical laboratory assistance at Dentalia by Katja Sampalahti, Oona Hällfors and Aija Koivusaari. They were always happy and helpful.

Adjunct professor Jorma Määttä for sharing scientific knowledge. M.Sc. Karoliina Kajander for discussions of science and for cooperation.

PhD Mirka Korhonen for inspiring me with her example and encouraging me to study natural sciences in my childhood.

All my friends, and especially Melissa, Mariina, Freya, Jaana, Roosa, Rosanne, Tuuli, Senni, for their friendship, without forgetting their big understanding that I have sometimes had to prioritize scientific work over social gatherings.

Finally, I would like to thank my family. My parents Minna and Timo for always supporting and believing in me. My sisters Anna and Silja (MD) for support, friendship and all our discussions of life. My little brothers Alvar and Eemeli for always sharing their cheerfulness. My love and best friend Tommi for all support, discussions of life and science, and understanding my working schedule.

Turku, August 2023
Saara Sirkkiä

References

- Abi-Rached, F. O., Martins, S. B., Campos, J. A., & Fonseca, R. G. (2014). Evaluation of roughness, wettability, and morphology of an yttria-stabilized tetragonal zirconia polycrystal ceramic after different airborne-particle abrasion protocols. *Journal of Prosthetic Dentistry*, *112*(6), 1385–1391. <https://doi.org/10.1016/j.prosdent.2014.07.005>
- Alliot-Licht, B., Gregoire, M., Orly, I., & Menanteau, J. (1991). Cellular activity of osteoblasts in the presence of hydroxyapatite: an in vitro experiment. *Biomaterials*, *199*(1), 752–756.
- AlMaimouni, Y. K., Benrashed, M. A., Alyousef, N. I., Shah, A. T., & Khan, A. S. (2020). Bioactive glass coated dental implants. *Dental Implants: Materials, Coatings, Surface Modifications and Interfaces with Oral Tissues*, 93–115. <https://doi.org/10.1016/B978-0-12-819586-4.00006-8>
- Anada, T., Kumagai, T., Honda, Y., Masuda, T., Kamijo, R., Kamakura, S., Yoshihara, N., Kuriyagawa, T., Shimauchi, H., & Suzuki, O. (2008). Dose-dependent osteogenic effect of octacalcium phosphate on mouse bone marrow stromal cells. *Tissue Engineering - Part A*, *14*(6), 965–978. <https://doi.org/10.1089/ten.tea.2007.0339>
- Anderson, J. M., Rodriguez, A., & Chang, D. T. (2008). Foreign body reaction to biomaterials. In *Seminars in Immunology* (Vol. 20, Issue 2, pp. 86–100). <https://doi.org/10.1016/j.smim.2007.11.004>
- Anna-Marja Säämänen, Terhi Heino, Jari Arokoski, Tero Järvinen, & Rami Korhonen. (2022). Tuki- ja liikuntaelämistön rakenne ja toiminta. In *Ortopedia* (pp. 13–48). Kandaattikustannus Oy.
- Baldwin, P., Li, D. J., Auston, D. A., Mir, H. S., Yoon, R. S., & Koval, K. J. (2019). Autograft, Allograft, and Bone Graft Substitutes: Clinical Evidence and Indications for Use in the Setting of Orthopaedic Trauma Surgery. *Journal of Orthopaedic Trauma*, *33*(4), 203–213. <https://doi.org/10.1097/BOT.0000000000001420>
- Ballo, A. M., Kokkari, A. K., Meretoja, V. V, Lassila, Lippo. L., Vallittu, P. K., & Närhi, T. O. (2008). Osteoblast proliferation and maturation on bioactive fiber-reinforced composite surface. *J Mater Sci: Mater Med*, *19*, 3169–3177. <https://doi.org/10.1007/s10856-008-3453-y>
- Beck, G. R., Ha, S. W., Camalier, C. E., Yamaguchi, M., Li, Y., Lee, J. K., & Weitzmann, M. N. (2012). Bioactive silica-based nanoparticles stimulate bone-forming osteoblasts, suppress bone-resorbing osteoclasts, and enhance bone mineral density in vivo. *Nanomedicine: Nanotechnology, Biology, and Medicine*, *8*(6), 793–803. <https://doi.org/10.1016/j.nano.2011.11.003>
- Bellido, T., Plotkin, L. I., & Bruzzaniti, A. (2019). Bone Cells. In *Basic and Applied Bone Biology* (pp. 37–55). Elsevier. <https://doi.org/10.1016/b978-0-12-813259-3.00003-8>
- Ben-Nissan, B. (2003). Natural bioceramics: From coral to bone and beyond. *Current Opinion in Solid State and Materials Science*, *7*(4–5), 283–288. <https://doi.org/10.1016/j.cossms.2003.10.001>
- Best, S. M., Porter, A. E., Thian, E. S., & Huang, J. (2008). Bioceramics: Past, present and for the future. *Journal of the European Ceramic Society*, *28*(7), 1319–1327. <https://doi.org/10.1016/j.jeurceramsoc.2007.12.001>
- Björkenheim, R., Strömberg, G., Ainola, M., Uppstu, P., Aalto-Setälä, L., Hupa, L., Pajarinen, J., & Lindfors, N. C. (2019). Bone morphogenic protein expression and bone formation are induced by bioactive glass S53P4 scaffolds in vivo. *Journal of Biomedical Materials Research - Part B Applied Biomaterials*, *107*(3), 847–857. <https://doi.org/10.1002/jbmb.34181>

- Bohner, M. (2000). Calcium orthophosphates in medicine: from ceramics to calcium phosphate cements. In *Int. J. Care Injured* (Vol. 3). www.elsevier.com/locate/injury
- Bohner, M., & Miron, R. J. (2019). A proposed mechanism for material-induced heterotopic ossification. In *Materials Today* (Vol. 22, pp. 132–141). Elsevier B.V. <https://doi.org/10.1016/j.mattod.2018.10.036>
- Bose, S., Fielding, G., Tarafder, S., Bandyopadhyay, A., & Keck, W. M. (2013). Understanding of dopant-induced osteogenesis and angiogenesis in calcium phosphate ceramics. *Trends in Biotechnology*, 31, 594–605. <https://doi.org/10.1016/j.tibtech.2013.06>
- Brauer, D. S., & Möncke, D. (2017). Chapter 3: Introduction to the Structure of Silicate, Phosphate and Borate Glasses. In *RSC Smart Materials* (Vols. 2017-January, Issue 23, pp. 61–88). Royal Society of Chemistry. <https://doi.org/10.1039/9781782622017-00061>
- Camilo, C. C., Silveira, C. A. E., Faeda, R. S., De Almeida Rollo, J. M. D., Purquerio, B. D. M., & Fortulan, C. A. (2017). Bone response to porous alumina implants coated with bioactive materials, observed using different characterization techniques. *Journal of Applied Biomaterials and Functional Materials*, 15(3), e223–e235. <https://doi.org/10.5301/jabfm.5000347>
- Campana, V., Milano, G., Pagano, E., Barba, M., Cicione, C., Salonna, G., Lattanzi, W., & Logroscino, G. (2014a). Bone substitutes in orthopaedic surgery: from basic science to clinical practice. *Journal of Materials Science: Materials in Medicine*, 25(10), 2445–2461. <https://doi.org/10.1007/s10856-014-5240-2>
- Campana, V., Milano, G., Pagano, E., Barba, M., Cicione, C., Salonna, G., Lattanzi, W., & Logroscino, G. (2014b). Bone substitutes in orthopaedic surgery: from basic science to clinical practice. *Journal of Materials Science: Materials in Medicine*, 25(10), 2445–2461. <https://doi.org/10.1007/s10856-014-5240-2>
- Cao, W., & Hench, L. L. (1996). Bioactive Materials. In *Ceramics International* (Vol. 22, Issue 95).
- Carrodeguas, R. G., & De Aza, S. (2011). α -Tricalcium phosphate: Synthesis, properties and biomedical applications. In *Acta Biomaterialia* (Vol. 7, Issue 10, pp. 3536–3546). Elsevier Ltd. <https://doi.org/10.1016/j.actbio.2011.06.019>
- Chevalier, J. (2006). What future for zirconia as a biomaterial? *Biomaterials*, 27(4), 535–543. <https://doi.org/10.1016/j.biomaterials.2005.07.034>
- Choi, G., Choi, A. H., Evans, L. A., Akyol, S., & Ben-Nissan, B. (2020). A review: Recent advances in sol-gel-derived hydroxyapatite nanocoatings for clinical applications. *Journal of the American Ceramic Society*, 103(10), 5442–5453. <https://doi.org/10.1111/jace.17118>
- Chróścicka, A., Jaegermann, Z., Wychowański, P., Ratajska, A., Sadło, J., Hoser, G., Michałowski, S., & Lewandowska-Szumiel, M. (2016). Synthetic Calcite as a Scaffold for Osteoinductive Bone Substitutes. *Annals of Biomedical Engineering*, 44(7), 2145–2157. <https://doi.org/10.1007/s10439-015-1520-3>
- Darvell, B. W. (2021). Bioactivity—Symphony or Cacophony? A Personal View of a Tangled Field. *Prosthesis*, 3(1), 75–84. <https://doi.org/10.3390/prosthesis3010008>
- Demers, C., Hamdy, C. R., Corsi, K., Chellat, F., Tabrizian, M., & Hocine Yahia, L. ' (2002). as a bone graft substitute: A review. In *Bio-Medical Materials and Engineering* (Vol. 12). IOS Press Natural coral exoskeleton.
- Eliaz, N., & Metoki, N. (2017). Calcium phosphate bioceramics: A review of their history, structure, properties, coating technologies and biomedical applications. *Materials*, 10(4). <https://doi.org/10.3390/ma10040334>
- El-Meliegy Emad, & van Noort Richard. (2012). Selection Criteria of Ceramics for Medical Applications. In *Glasses and Glass Ceramics for Medical Applications* (1st ed., pp. 19–26). Springer New York, NY. <https://doi.org/https://doi.org/10.1007/978-1-4614-1228-1>
- Fagerlund, S., Ek, P., Hupa, L., & Hupa, M. (2012). Dissolution kinetics of a bioactive glass by continuous measurement. *Journal of the American Ceramic Society*, 95(10), 3130–3137. <https://doi.org/10.1111/j.1551-2916.2012.05374.x>

- Fagerlund, S., & Hupa, L. (2017). Chapter 1: Melt-derived Bioactive Silicate Glasses. In *RSC Smart Materials* (Vols. 2017-January, Issue 23, pp. 1–26). Royal Society of Chemistry. <https://doi.org/10.1039/9781782622017-00001>
- Fagerlund, S., Hupa, L., & Hupa, M. (2013). Dissolution patterns of biocompatible glasses in 2-Amino-2-hydroxymethyl- propane-1,3-diol (Tris) buffer. *Acta Biomaterialia*, *9*(2), 5400–5410. <https://doi.org/10.1016/j.actbio.2012.08.051>
- Fu, K., Xu, Q., Czernuszka, J., Triffitt, J. T., & Xia, Z. (2013). Characterization of a biodegradable coralline hydroxyapatite/calcium carbonate composite and its clinical implementation. *Biomedical Materials*, *8*(6), 065007. <https://doi.org/10.1088/1748-6041/8/6/065007>
- Galvão Ribeiro, B. R., Galvão Rabelo Caldas, M. R., Almeida, A. A., Fonseca, R. G., & Adabo, G. L. (2018). Effect of surface treatments on repair with composite resin of a partially monoclinic phase transformed yttrium-stabilized tetragonal zirconia. *Journal of Prosthetic Dentistry*, *119*(2), 286–291. <https://doi.org/10.1016/j.prosdent.2017.02.014>
- Goldberg, V. M., & Akhavan, S. (2005). *4 Biology of Bone Grafts*.
- Gopal, V., & Manivasagam, G. (2018). Zirconia-alumina composite for orthopedic implant application. In *Applications of Nanocomposite Materials in Orthopedics* (pp. 201–219). Elsevier. <https://doi.org/10.1016/B978-0-12-813740-6.00011-9>
- Habibovic, P., & Barralet, J. E. (2011). Bioinorganics and biomaterials: Bone repair. In *Acta Biomaterialia* (Vol. 7, Issue 8, pp. 3013–3026). Elsevier Ltd. <https://doi.org/10.1016/j.actbio.2011.03.027>
- Hayashi, K., Munar, M. L., & Ishikawa, K. (2020). Effects of macropore size in carbonate apatite honeycomb scaffolds on bone regeneration. *Materials Science and Engineering C*, *111*. <https://doi.org/10.1016/j.msec.2020.110848>
- Hench, L. L. (1991). Bioceramics: From Concept to Clinic. *Journal of the American Ceramic Society*, *74*(7), 1487–1510. <https://doi.org/10.1111/j.1151-2916.1991.tb07132.x>
- Hench, L. L. (2009). Genetic design of bioactive glass. *Journal of the European Ceramic Society*, *29*(7), 1257–1265. <https://doi.org/10.1016/j.jeurceramsoc.2008.08.002>
- Hench, L. L., & Andersson, Ö. (1993). Bioactive glasses. In *An Introduction to Bioceramics* (pp. 41–62). WORLD SCIENTIFIC. https://doi.org/10.1142/9789814317351_0003
- Hjerpe, J., Närhi, T. O., Vallittu, P. K., & Lassila, L. V. J. (2016). Surface roughness and the flexural and bend strength of zirconia after different surface treatments. *Journal of Prosthetic Dentistry*, *116*(4), 577–583. <https://doi.org/10.1016/j.prosdent.2016.02.018>
- Hoppe, A., Güldal, N. S., & Boccaccini, A. R. (2011). A review of the biological response to ionic dissolution products from bioactive glasses and glass-ceramics. In *Biomaterials* (Vol. 32, Issue 11, pp. 2757–2774). <https://doi.org/10.1016/j.biomaterials.2011.01.004>
- Horie, M., Nishio, K., Kato, H., Endoh, S., Fujita, K., Nakamura, A., Kinugasa, S., Hagihara, Y., Yoshida, Y., & Iwahashi, H. (2014). Evaluation of cellular influences caused by calcium carbonate nanoparticles. *Chemico-Biological Interactions*, *210*(1), 64–76. <https://doi.org/10.1016/j.cbi.2013.12.013>
- Hupa, L. (2018). Composition-property relations of bioactive silicate glasses. In *Bioactive Glasses* (pp. 1–35). Elsevier. <https://doi.org/10.1016/b978-0-08-100936-9.00001-0>
- Ishikawa, K. (2019). Carbonate apatite bone replacement: Learn from the bone. *Journal of the Ceramic Society of Japan*, *127*(9), 595–601. <https://doi.org/10.2109/jcersj2.19042>
- Jamali, A., Hilpert, A., Debes, J., Afshar, P., Rahban, S., & Holmes, R. (2002). Hydroxyapatite/calcium carbonate (HA/CC) vs. plaster of Paris: A histomorphometric and radiographic study in a rabbit tibial defect model. *Calcified Tissue International*, *71*(2), 172–178. <https://doi.org/10.1007/s00223-001-1087-x>
- Joe, I. H., Vasudevan, A. K., Aruldas, G., Damodaran, A. D., & Warriar, K. G. K. (1997). BRIEF COMMUNICATION - FTIR as a Tool to Study High-Temperature Phase Formation in Sol–Gel Aluminium Titanate. In *JOURNAL OF SOLID STATE CHEMISTRY* (Vol. 131).

- Jones, J. R., Brauer, D. S., Hupa, L., & Greenspan, D. C. (2016). Bioglass and Bioactive Glasses and Their Impact on Healthcare. *International Journal of Applied Glass Science*, 7(4), 423–434. <https://doi.org/10.1111/ijag.12252>
- Khan, A. A., Mohamed, B. A., Mirza, E. H., Syed, J., Divakar, D. D., & Vallittu, P. K. (2019). Surface wettability and nano roughness at different grit blasting operational pressures and their effects on resin cement to zirconia adhesion. *Dental Materials Journal*, 38(3), 388–395. <https://doi.org/10.4012/dmj.2018-137>
- Kim, E. J., Bu, S. Y., Sung, M. K., & Choi, M. K. (2013). Effects of silicon on osteoblast activity and bone mineralization of MC3T3-E1 cells. *Biological Trace Element Research*, 152(1), 105–112. <https://doi.org/10.1007/s12011-012-9593-4>
- Kim, T., See, C. W., Li, X., & Zhu, D. (2020). Orthopedic implants and devices for bone fractures and defects: Past, present and perspective. *Engineered Regeneration*, 1, 6–18. <https://doi.org/10.1016/j.engreg.2020.05.003>
- Levy, C. L., Matthews, G. P., Laudone, G. M., Beckett, S., Turner, A., Schoelkopf, J., & Gane, P. A. C. (2017). Mechanism of adsorption of actives onto microporous functionalised calcium carbonate (FCC). *Adsorption*, 23(4), 603–612. <https://doi.org/10.1007/s10450-017-9880-7>
- Li, X., Yang, X., Liu, X., He, W., Huang, Q., Li, S., & Feng, Q. (2018). Calcium carbonate nanoparticles promote osteogenesis compared to adipogenesis in human bone-marrow mesenchymal stem cells. *Progress in Natural Science: Materials International*, 28(5), 598–608. <https://doi.org/10.1016/j.pnsc.2018.09.004>
- Lieberman, J. R., Friedlaender, G. E., Joneschild, E., & Urbaniak, J. R. (2005). *6 Biology of the Vascularized Fibular Graft*.
- Lindfors, N., Romano, C., Scarponi, S., Lorenzo, D., Monica, B., Frantzen, J., De Veij Mestdagh, P. D., Colnot, D. R., Borggreven, P. A., & Quak, J. J. (2017). Chapter 14: Bioactive Glasses in Infection Treatment. In *RSC Smart Materials* (Vols. 2017-January, Issue 23, pp. 316–335). Royal Society of Chemistry. <https://doi.org/10.1039/9781782622017-00316>
- Lohmann, C. H., Schwartz, Z., Kok, G., Jahn, U., Buchhorn, G. H., Macdougall, M. J., Casasola, D., Liu, Y., Sylvia, V. L., Dean, D. D., & Boyan, B. D. (2000). Phagocytosis of wear debris by osteoblasts affects differentiation and local factor production in a manner dependent on particle composition. *Biomaterials*, 21, 551–561.
- Maçon, A. L. B., Kim, T. B., Valliant, E. M., Goetschius, K., Brow, R. K., Day, D. E., Hoppe, A., Boccaccini, A. R., Kim, I. Y., Ohtsuki, C., Kokubo, T., Osaka, A., Vallet-Regí, M., Arcos, D., Fraile, L., Salinas, A. J., Teixeira, A. V., Vueva, Y., Almeida, R. M., ... Jones, J. R. (2015). A unified in vitro evaluation for apatite-forming ability of bioactive glasses and their variants. *Journal of Materials Science: Materials in Medicine*, 26(2), 1–10. <https://doi.org/10.1007/s10856-015-5403-9>
- Madupalli, H., Pavan, B., & Tecklenburg, M. M. J. (2017). Carbonate substitution in the mineral component of bone: Discriminating the structural changes, simultaneously imposed by carbonate in A and B sites of apatite. *Journal of Solid State Chemistry*, 255, 27–35. <https://doi.org/10.1016/j.jssc.2017.07.025>
- Manicone, P. F., Rossi Iommetti, P., & Raffaelli, L. (2007). An overview of zirconia ceramics: Basic properties and clinical applications. In *Journal of Dentistry* (Vol. 35, Issue 11, pp. 819–826). <https://doi.org/10.1016/j.jdent.2007.07.008>
- Marsell, R., & Einhorn, T. A. (2011). The biology of fracture healing. *Injury*, 42(6), 551–555. <https://doi.org/10.1016/j.injury.2011.03.031>
- Martins, S. B., Abi-Rached, F. de O., Adabo, G. L., Baldissara, P., & Fonseca, R. G. (2019). Influence of Particle and Air-Abrasion Moment on Y-TZP Surface Characterization and Bond Strength. *Journal of Prosthodontics*, 28(1), e271–e278. <https://doi.org/10.1111/jopr.12718>
- Masson, B. (2009). Emergence of the alumina matrix composite in total hip arthroplasty. *International Orthopaedics*, 33(2), 359–363. <https://doi.org/10.1007/s00264-007-0484-9>

- Matinlinna, J. P., & Lassila, L. (2004). *Article in The International journal of prosthodontics*. <https://www.researchgate.net/publication/8585276>
- McEntire, B. J., Bal, B. S., Rahaman, M. N., Chevalier, J., & Pezzotti, G. (2015). Ceramics and ceramic coatings in orthopaedics. *Journal of the European Ceramic Society*, 35(16), 4327–4369. <https://doi.org/10.1016/j.jeurceramsoc.2015.07.034>
- Mladenović, Ž., Johansson, A., Willman, B., Shahabi, K., Björn, E., & Ransjö, M. (2014). Soluble silica inhibits osteoclast formation and bone resorption in vitro. *Acta Biomaterialia*, 10(1), 406–418. <https://doi.org/10.1016/j.actbio.2013.08.039>
- Moerke, C., Mueller, P., & Nebe, B. (2016). Attempted caveolae-mediated phagocytosis of surface-fixed micro-pillars by human osteoblasts. *Biomaterials*, 76, 102–114. <https://doi.org/10.1016/j.biomaterials.2015.10.030>
- Monchau, F., Hivart, P., Genestie, B., Chai, F., Descamps, M., & Hildebrand, H. F. (2013). Calcite as a bone substitute. Comparison with hydroxyapatite and tricalcium phosphate with regard to the osteoblastic activity. *Materials Science and Engineering C*, 33(1), 490–498. <https://doi.org/10.1016/j.msec.2012.09.019>
- Monfoulet, L. E., Becquart, P., Marchat, D., Vandamme, K., Bourguignon, M., Pacard, E., Viateau, V., Petite, H., & Logeart-Avramoglou, D. (2014). The pH in the microenvironment of human mesenchymal stem cells is a critical factor for optimal osteogenesis in tissue-engineered constructs. *Tissue Engineering - Part A*, 20(13–14), 1827–1840. <https://doi.org/10.1089/ten.tea.2013.0500>
- Nasar, A. (2019). Hydroxyapatite and its coatings in dental implants. *Applications of Nanocomposite Materials in Dentistry*, 145–160. <https://doi.org/10.1016/B978-0-12-813742-0.00008-0>
- Nommeots-Nomm, A., Hupa, L., Rohanová, D., & Brauer, D. S. (2020). A review of acellular immersion tests on bioactive glasses—influence of medium on ion release and apatite formation. *International Journal of Applied Glass Science*, 11(3), 537–551. <https://doi.org/10.1111/ijag.15006>
- Omidi, M., Fatehinya, A., Farahani, M., Akbari, Z., Shahmoradi, S., Yazdian, F., Tahiri, M., Moharamzadeh, K., Tayebi, L., & Vashae, D. (2017). Characterization of biomaterials. *Biomaterials for Oral and Dental Tissue Engineering*, 97–115. <https://doi.org/10.1016/B978-0-08-100961-1.00007-4>
- Ong, J. C. Y., Kennedy, M. T., Mitra, A., & Harty, J. A. (2012). Fixation of tibial plateau fractures with synthetic bone graft versus natural bone graft: A comparison study. *Irish Journal of Medical Science*, 181(2), 247–252. <https://doi.org/10.1007/s11845-011-0797-y>
- Oonishi Jr, H., Oonishi, H., Ohashi, H., Kawahara, I., Hanaoka, Y., Iwata, R., Hench, L. L., Oonishi Jr, H., Oonishi, H., Kawahara, I., Hanaoka, Y., Ohashi, H., Iwata, R., & Hench, L. (2014). Clinical Applications of Hydroxyapatite in Orthopedics. *Advances in Calcium Phosphate Biomaterials*, 19–49. https://doi.org/10.1007/978-3-642-53980-0_2
- Özcan, M., & Vallittu, P. K. (2003). Effect of surface conditioning methods on the bond strength of luting cement to ceramics. *Dental Materials*, 19(8), 725–731. [https://doi.org/10.1016/S0109-5641\(03\)00019-8](https://doi.org/10.1016/S0109-5641(03)00019-8)
- Pabbruwe, M. B., Standard, O. C., Sorrell, C. C., & Howlett, C. R. (2004). Effect of silicon doping on bone formation within alumina porous domains. *Journal of Biomedical Materials Research - Part A*, 71(2), 250–257. <https://doi.org/10.1002/jbm.a.30154>
- Pan, H., Zhao, X., Darvell, B. W., & Lu, W. W. (2010). Apatite-formation ability - Predictor of “bioactivity”? In *Acta Biomaterialia* (Vol. 6, Issue 11, pp. 4181–4188). Elsevier Ltd. <https://doi.org/10.1016/j.actbio.2010.05.013>
- Perrichon, A., Liu, B., Chevalier, J., Gremillard, L., Reynard, B., Farizon, F., Liao, J.-D., & Geringer, J. (2017). Ageing, Shocks and Wear Mechanisms in ZTA and the Long-Term Performance of Hip Joint Materials. *Materials*, 10(6), 569. <https://doi.org/10.3390/ma10060569>
- Rahmati, M., & Mozafari, M. (2019). Biocompatibility of alumina-based biomaterials—A review. In *Journal of Cellular Physiology* (Vol. 234, Issue 4, pp. 3321–3335). Wiley-Liss Inc. <https://doi.org/10.1002/jcp.27292>

- Reddy, S., Dischino, M., & Soslowsky, L. J. (2009). Biomechanics-Part i. In *Bone Pathology* (pp. 61–68). Humana Press. https://doi.org/10.1007/978-1-59745-347-9_3
- Rehman, I., & Bonfield, W. (1997). Characterization of hydroxyapatite and carbonated apatite by photo acoustic FTIR spectroscopy. In *JOURNAL OF MATERIALS SCIENCE: MATERIALS IN MEDICINE* (Vol. 8).
- Ripamonti, U., Crooks, J., Khoali, L., & Roden, L. (2009). The induction of bone formation by coral-derived calcium carbonate/hydroxyapatite constructs. *Biomaterials*, *30*(7), 1428–1439. <https://doi.org/10.1016/j.biomaterials.2008.10.065>
- Roeder, R. K. (2013). Mechanical Characterization of Biomaterials. In *Characterization of Biomaterials* (pp. 49–104). Elsevier Inc. <https://doi.org/10.1016/B978-0-12-415800-9.00003-6>
- Roth, R. (2019). *Functionalized calcium carbonate based peptide formulation: Aspects of the development for oral delivery to the buccal and intestinal mucosa*.
- Safadi, F. F., Barbe, M. F., Abdelmagid, S. M., Rico, M. C., Aswad, R. A., Litvin, J., & Popoff, S. N. (2009). Bone structure, development and bone biology. In *Bone Pathology* (pp. 1–50). Humana Press. https://doi.org/10.1007/978-1-59745-347-9_1
- Samavedi, S., Whittington, A. R., & Goldstein, A. S. (2013). Calcium phosphate ceramics in bone tissue engineering: A review of properties and their influence on cell behavior. In *Acta Biomaterialia* (Vol. 9, Issue 9, pp. 8037–8045). Elsevier Ltd. <https://doi.org/10.1016/j.actbio.2013.06.014>
- Sampath Kumar, T. S. (2013). Physical and Chemical Characterization of Biomaterials. In *Characterization of Biomaterials* (pp. 11–47). Elsevier Inc. <https://doi.org/10.1016/B978-0-12-415800-9.00002-4>
- Schemitsch, E. H. (2017). Size Matters: Defining Critical in Bone Defect Size! *Journal of Orthopaedic Trauma*, *31*, S20–S22. <https://doi.org/10.1097/BOT.0000000000000978>
- Serra, J., González, P., Liste, S., Serra, C., Chiussi, S., León, B., Pérez-Amor, M., Ylänen, H. O., & Hupa, M. (2003). FTIR and XPS studies of bioactive silica based glasses. *Journal of Non-Crystalline Solids*, *332*(1–3), 20–27. <https://doi.org/10.1016/j.jnoncrysol.2003.09.013>
- Sfeir, C., Ho, L., Doll, B. A., Azari, K., & Hollinger, J. O. (2005). *2 Fracture Repair*.
- Shanmugam, K., & Sahadevan, R. (2018). Bioceramics-An introductory overview. In *Fundamental Biomaterials: Ceramics* (pp. 1–46). Elsevier Inc. <https://doi.org/10.1016/B978-0-08-102203-0.00001-9>
- Sun, J.-S., Liu, H.-C., Hong-Shong Chang, W., Li, J., Lin, F.-H., & Tai, H.-C. (1998). Influence of hydroxyapatite particle size on bone cell activities: An in vitro study. In *J Biomed Mater Res* (Vol. 39).
- Thammajaruk, P., Buranadham, S., Thanatvarakorn, O., & Guazzato, M. (2018). Influence of nano-structured alumina coating on composite-zirconia bonding and its characterization. *The Journal of Adhesive Dentistry*, *20*(3), 233–242. <https://doi.org/10.3290/j.jad.a40512>
- Thasneem, Y. M., & Sharma, C. P. (2013). In Vitro Characterization of Cell-Biomaterials Interactions. In *Characterization of Biomaterials* (pp. 175–205). Elsevier Inc. <https://doi.org/10.1016/B978-0-12-415800-9.00005-X>
- Uribe, P., Johansson, A., Jugdaohsingh, R., Powell, J. J., Magnusson, C., Davila, M., Westerlund, A., & Ransjö, M. (2020). Soluble silica stimulates osteogenic differentiation and gap junction communication in human dental follicle cells. *Scientific Reports*, *10*(1). <https://doi.org/10.1038/s41598-020-66939-1>
- Vallittu, P. K. (2017). Bioactive glass-containing cranial implants: an overview. *Journal of Materials Science*, *52*(15), 8772–8784. <https://doi.org/10.1007/s10853-017-0888-x>
- Vallittu, P. K., Närhi, T. O., & Hupa, L. (2015). Fiber glass-bioactive glass composite for bone replacing and bone anchoring implants. In *Dental Materials* (Vol. 31, Issue 4, pp. 371–381). Elsevier Inc. <https://doi.org/10.1016/j.dental.2015.01.003>
- Vallittu, P. K., Posti, J. P., Piitulainen, J. M., Serlo, W., Määttä, J. A., Heino, T. J., Pagliari, S., Syrjänen, S. M., & Forte, G. (2020). Biomaterial and implant induced ossification: in vitro and in vivo

- findings. *Journal of Tissue Engineering and Regenerative Medicine*, 14(8), 1157–1168. <https://doi.org/10.1002/term.3056>
- Wall, V., Nguyen, T.-H., Nguyen, N., & Tran, P. A. (2021). *biomedicines Controlling Antibiotic Release from Polymethylmethacrylate Bone Cement*. <https://doi.org/10.3390/biomedicines>
- Walsh, W. R., Chapman-Sheath, P. J., Cain, S., Debes, J., Bruce, W. J. M., Svehla, M. J., & Gillies, R. M. (2003). A resorbable porous ceramic composite bone graft substitute in a rabbit metaphyseal defect model. In *Journal of Orthopaedic Research* (Vol. 21, Issue 4, pp. 655–661). Elsevier BV. [https://doi.org/10.1016/S0736-0266\(03\)00012-3](https://doi.org/10.1016/S0736-0266(03)00012-3)
- Wang, H., & Chu, P. K. (2013). Surface Characterization of Biomaterials. In *Characterization of Biomaterials* (pp. 105–174). Elsevier Inc. <https://doi.org/10.1016/B978-0-12-415800-9.00004-8>
- Wang, L., Wang, C., Wu, S., Fan, Y., & Li, X. (2020). Influence of the mechanical properties of biomaterials on degradability, cell behaviors and signaling pathways: Current progress and challenges. In *Biomaterials Science* (Vol. 8, Issue 10, pp. 2714–2733). Royal Society of Chemistry. <https://doi.org/10.1039/d0bm00269k>
- Wang, W., & Yeung, K. W. K. (2017). Bone grafts and biomaterials substitutes for bone defect repair: A review. In *Bioactive Materials* (Vol. 2, Issue 4, pp. 224–247). KeAi Communications Co. <https://doi.org/10.1016/j.bioactmat.2017.05.007>
- Wong, C. S. (2021). Surface and biological characterization of biomaterials. *Structural Biomaterials: Properties, Characteristics, and Selection*, 33–66. <https://doi.org/10.1016/B978-0-12-818831-6.00002-1>
- Zhang, D., Leppäranta, O., Munukka, E., Ylänen, H., Viljanen, M. K., Eerola, E., Hupa, M., & Hupa, L. (2010). Antibacterial effects and dissolution behavior of six bioactive glasses. *Journal of Biomedical Materials Research - Part A*, 93(2), 475–483. <https://doi.org/10.1002/jbm.a.32564>
- Zheng, K., Solodovnyk, A., Li, W., Goudouri, O. M., Stähli, C., Nazhat, S. N., & Boccaccini, A. R. (2015). Aging time and temperature effects on the structure and bioactivity of gel-derived 45S5 glass-ceramics. *Journal of the American Ceramic Society*, 98(1), 30–38. <https://doi.org/10.1111/jace.13258>
- Zhou, X., Zhang, N., Mankoci, S., & Sahai, N. (2017). Silicates in orthopedics and bone tissue engineering materials. In *Journal of Biomedical Materials Research - Part A* (Vol. 105, Issue 7, pp. 2090–2102). John Wiley and Sons Inc. <https://doi.org/10.1002/jbm.a.36061>



**TURUN
YLIOPISTO**
UNIVERSITY
OF TURKU

ISBN 978-951-29-9525-7 (PRINT)
ISBN 978-951-29-9526-4 (PDF)
ISSN 0355-9483 (Print)
ISSN 2343-3213 (Online)

